AGU ADVANCING EARTH AND SPACE SCIENCE

Water Resources Research

RESEARCH ARTICLE
10.1029/2021WR031781

Bedrock Vadose Zone Storage Dynamics Under Extreme Drought: Consequences for Plant Water Availability, Recharge, and Runoff

W. J. Hahm[1], D. N. Dralle[2], M. Sanders[3], A. B. Bryk[4], K. E. Fauria[5], M. H. Huang[6], B. Hudson-Rasmussen[6], M. D. Nelson[7], M. A. Pedrazas[7], L. Schmidt[7], J. Whiting[2], W. E. Dietrich[4], and D. M. Rempe[7]

[1]Department of Geography, Simon Fraser University, Burnaby, BC, Canada, [2]Pacific Southwest Research Station, USDA Forest Service, Albany, CA, USA, [3]Department of Earth Sciences, University of Oregon, Eugene, OR, USA, [4]Department of Earth and Planetary Science, University of California-Berkeley, Berkeley, CA, USA, [5]Department of Earth and Environmental Sciences, Vanderbilt University, Nashville, TN, USA, [6]Department of Geology, University of Maryland, College Park, MD, USA, [7]Department of Geological Sciences, University of Texas-Austin, Austin, TX, USA

Key Points:

- Multi-year field study reveals role of deep bedrock moisture within hillslopes
- Large deep storage capacity relative to precipitation in dry years drives variable interannual storage
- Drought reduced rock moisture replenishment, groundwater recharge, streamflow, and blue oak water potential, transpiration and leaf area

Correspondence to:
W. J. Hahm,
whahm@sfu.ca

Citation:
Hahm, W. J., Dralle, D. N., Sanders, M., Bryk, A. B., Fauria, K. E., Huang, M. H., et al. (2022). Bedrock vadose zone storage dynamics under extreme drought: Consequences for plant water availability, recharge, and runoff. *Water Resources Research*, *58*, e2021WR031781. https://doi.org/10.1029/2021WR031781

Received 14 DEC 2021
Accepted 4 APR 2022

Abstract Bedrock vadose zone water storage (i.e., rock moisture) dynamics are rarely observed but potentially key to understanding drought responses. Exploiting a borehole network at a Mediterranean blue oak savanna site—Rancho Venada—we document how water storage capacity in deeply weathered bedrock profiles regulates woody plant water availability and groundwater recharge. The site is in the Northern California Coast Range within steeply dipping turbidites. In a wet year (water year 2019; 647 mm of precipitation), rock moisture was quickly replenished to a characteristic storage capacity, recharging groundwater that emerged at springs to generate streamflow. In the subsequent rainless summer growing season, rock moisture was depleted by about 93 mm. In two drought years that followed (212 and 121 mm of precipitation) the total amount of rock moisture gained each winter was about 54 and 20 mm, respectively, and declines were documented exceeding these amounts, resulting in progressively lower rock moisture content. Oaks, which are rooted into bedrock, demonstrated signs of water stress in drought, including reduced transpiration rates and extremely low water potentials. In the 2020–2021 drought, precipitation did not exceed storage capacity, resulting in variable belowground water storage, increased plant water stress, and no recharge or runoff. Rock moisture deficits (rather than soil moisture deficits) explain these responses.

Plain Language Summary When rainfall is lower than normal, water stored belowground can sustain forests and drain to streams. Does the presence of deep, dynamic water storage in bedrock below soil provide enhanced drought resilience? We used a network of deep boreholes drilled into hillslopes to study how the weathered bedrock unsaturated zone acts as a water source for woody vegetation and mediates groundwater recharge. At our winter-wet, summer-dry oak savanna field site in the Northern California Coast Range, dry season reductions in rock moisture were driven by woody plant water use. However, the water storage capacity of the subsurface exceeded net precipitation inputs in dry winters. Thus, deep water storage was not replenished during an extreme drought to the same degree as in wetter years, resulting in decreased groundwater recharge and streamflow, and lower water availability for trees—even those deeply rooted in the bedrock. Trees using bedrock-water exhibited dieback in the second year of the hot, dry 2020–2021 drought. These findings motivate expanded study of how moisture storage properties of deep bedrock influence the susceptibility of vegetation to drought over multiple years.

1. Introduction

Meteorological droughts have recently intensified in many regions and are anticipated to continue to increase in frequency and severity under future climate (Swain et al., 2018; Tramblay et al., 2020; C. Wu et al., 2020). This shift will impact groundwater recharge, streamflow initiation and baseflow, and increase the frequency of municipal water shortages and flow reductions that negatively impact aquatic ecosystems. Droughts can trigger dramatic plant community responses like sudden mass mortality events (which are often followed by or associated with fire; Allen et al., 2010). Although insects and land use history (including fire exclusion) contribute to these events, plant water stress is fundamentally mediated by subsurface water supply and atmospheric water demand (Breshears et al., 2013; Choat et al., 2018; Williams et al., 2013). In spite of extensive efforts to better understand

physiological response to water availability, predicting tree mortality in meteorological drought remains challenging (L. D. L. Anderegg et al., 2013; Steinkamp & Hickler, 2015; Trugman et al., 2021).

We are limited by our lack of understanding of how subsurface water storage capacity influences how climate mediates water storage dynamics. This in turn hinders our ability to predict where the subsurface will buffer terrestrial hydrologic processes, including recharge and streamflow, from meteorological drought. Many forests and water resources are concentrated in upland landscapes (Immerzeel et al., 2020), where subsurface water storage capacity is controlled by the extent of weathering (e.g., Graham et al., 2010; Hahm, Rempe, et al., 2019; Klos et al., 2018; Rempe & Dietrich, 2018). The propagation of chemical and physical weathering fronts downward into fresh bedrock (chemically unaltered bedrock parent material) creates the subsurface critical zone (e.g., Riebe et al., 2017). This zone typically consists of relatively thin soils (<1 m (Amundson et al., 2015))—whose properties have been systematically documented for decades as part of widespread mapping efforts—and underlying weathered bedrock (in situ material that exhibits chemical alteration and/or physical fracturing and dilation), which can be tens of meters thick and whose properties remain undocumented at large spatial scales. Poor understanding of the depth extent and water storage dynamics of weathered bedrock is due largely to accessibility challenges (direct observations are typically limited to road/stream-cuts, drilling or landslides) and a historical focus on soil as the life-sustaining layer mantling Earth's terrestrial surface. Nevertheless, woody plant communities are widespread on landscapes with thin soil underlain by weathered bedrock (McCormick et al., 2021; Wald et al., 2013), and numerous field-based studies have documented root presence in and/or plant extraction of water from weathered bedrock (Anderson et al., 1995; Arkley, 1981; Hahm et al., 2020; Hubbert et al., 2001; Lewis & Burgy, 1964; Miller et al., 2010; Rempe & Dietrich, 2018; Rose et al., 2003; Zwieniecki & Newton, 1996). This deep water-root-rock interaction has important consequences for transpiration, groundwater recharge, streamflow, landscape evolution and the carbon cycle (Brantley et al., 2017; Dawson et al., 2020; Schwinning, 2020; Tune et al., 2020). Under some forests, seasonal moisture storage in the weathered bedrock vadose zone (rock moisture) has been shown to be larger than seasonal soil moisture and (saturated) groundwater storage (Dralle et al., 2018; Rempe & Dietrich, 2018). This deep unsaturated moisture dynamic mediates—and is driven by—plant water uptake (Anderson et al., 1995; Crouchet et al., 2019; Ding et al., 2020; Hahm et al., 2020; Nardini et al., 2020; Rempe & Dietrich, 2018; Rose et al., 2003), and has recently been implicated as determining the fate of ecosystems in drought (Goulden & Bales, 2019; McDowell et al., 2019). However, most studies to date have identified the role of bedrock moisture via inference (e.g., water flux tracking (McCormick et al., 2021), isotopic signatures (Z. Wu et al., 2021), or modeling (Mackay et al., 2020; Tague & Moritz, 2019)), rather than direct observation.

How should subsurface water storage capacity (in both soil and weathered bedrock) mediate water availability to plants and streams? Mediterranean ecosystems are storage-dominated systems, because water supply and demand are out of phase. This means that dry season water supply—for both plants and streams—comes from water stored in prior wet seasons, underscoring the importance of subsurface storage capacity (Anderson et al., 1995; Arkley, 1981; Ichii et al., 2009; Rose et al., 2003). Total water storage capacity describes the maximum amount of water that can be stored below ground, and is limited by total available porosity (e.g., Klos et al., 2018). Plant-available water storage capacity—of primary interest here—is constrained by the total water storage capacity. Modeling and field evidence suggest that in locations where net wet season rainfall (winter precipitation minus interception and evapotranspiration) is always larger than the plant-available subsurface water storage capacity, storage will be replenished to capacity in both relatively wet and dry (drought) years (Fellows & Goulden, 2017; Hahm, Dralle, et al., 2019; Rempe & Dietrich, 2018; Milly, 1994; Smith et al., 2011). This situation—termed storage capacity limitation—can result in a decoupling of summer dry season plant water availability from annual precipitation totals (Hahm, Dralle, et al., 2019). Under storage capacity limited conditions, storage capacity (and not precipitation) limits the amount of seasonal water storage, and dry season water availability is uncorrelated with annual precipitation, which may effectively shield ecosystems from meteorological drought. In addition to storage capacity, which sets the upper bound on seasonally dynamic storage, the actual storage used in a given year is also determined by energy availability and the presence of roots to extract water (Fellows & Goulden, 2017; Goulden & Bales, 2019; Hahm et al., 2020; Klos et al., 2018; Rempe & Dietrich, 2018; Roche et al., 2020).

Precipitation in excess of storage capacity generally leaves catchments intra-seasonally as streamflow in rain-dominated Mediterranean climates (Sayama et al., 2011). In contrast, at locations where large water storage capacity relative to precipitation enables large water storage deficits, net wet season precipitation may be too low to

replenish plant-available water storage, and therefore precipitation—not storage capacity—can limit the amount of seasonal water storage. In this context, deficits refer to the difference between actual storage and the maximum storage capacity. These end-member possibilities (storage capacity limitation vs. precipitation limitation) generate testable hypotheses regarding plant sensitivity to meteorological drought. At seven storage-capacity limited sites (where precipitation was always greater than storage capacity, even in dry years) in California, Hahm, Dralle, et al. (2019) showed that dry season plant greenness was uncorrelated with the preceding wet season's total rainfall. These sites could be considered stable hydrologic refugia, in the sense of McLaughlin et al. (2017), and did not experience significant tree dieback in spite of greater than twofold precipitation reductions in the 2011–2016 drought that killed more than a hundred million trees across the state (USFS, 2016). At precipitation-limited sites (where typical net precipitation input may be less than storage capacity), plant transpiration and growth in the dry season should be coupled to the preceding wet season rainfall, and therefore sensitive to meteorological drought (Nourtier et al., 2014). Although the preceding framework arises from considerations of winter-wet, summer-dry Mediterranean climates, the relative magnitude of precipitation versus storage capacity also emerges as a key dimensionless variable controlling the distribution of plant water availability in stochastic models that do not require rainfall seasonality (Laio et al., 2001; Milly, 1994; Porporato et al., 2004; Zanardo et al., 2012).

The winter-wet, summer-dry ecohydrologic framework makes parallel predictions about related terrestrial hydrologic processes: At precipitation-limited sites, groundwater recharge and streamflow may not increase in relatively dry wet seasons, as infiltrating precipitation may only be sufficient to partially replenish storage deficits in the soil and weathered bedrock vadose zone, failing to trigger drainage to water tables that drive streamflow (Dralle et al., 2018). In contrast, at storage-capacity limited sites, wet season increases in recharge and streamflow will occur even in drought, although the total amount of runoff will scale with the amount of precipitation in excess of the storage deficit (Hahm, Dralle, et al., 2019).

Storage capacity-centered ecohydrologic frameworks share process elements with the conditions of "overshoot" and "overdraft", which have both been implicated recently in tree mortality events triggered by drought. Overshoot describes the condition in which plant growth is promoted during favorable periods (in this context, relatively wet winters), but the demand for water by the plant community is not met in subsequent unfavorable periods (e.g., a dry winter which fails to replenish the storage deficit; Jump et al., 2017). This is consistent with the precipitation-limited end-member condition described above. Overdraft has been used to describe the condition in which evapotranspiration exceeds precipitation over a multi-year period, which similarly results in net drawdowns of subsurface water storage during meteorological drought (Goulden & Bales, 2019). Such conditions would also fit under the precipitation-limited end-member condition, as net winter precipitation during periods of overdraft is insufficient to replenish storage deficits, and is therefore less than the storage capacity.

Based on these considerations, we anticipate that precipitation-limited conditions are likely to be inherently sensitive to meteorological drought, in contrast to storage-capacity limited conditions. This motivates the study of subsurface water storage dynamics at precipitation-limited field sites. Here, we study a site that we anticipated to be precipitation-limited (i.e., large storage capacity relative to rainfall) based on its semi-arid climate and prior observations of a deep bedrock weathering front (Pedrazas et al., 2021). We monitored moisture dynamics across an existing network of deep boreholes that penetrate deeply weathered bedrock profiles under a semi-arid blue oak (*Quercus douglasii*) savanna. We hypothesized that a coupling should exist between inter-annual rainfall variability, subsurface moisture dynamics, and ecosystem water availability. The site, like the rest of the Mediterranean climate zone of California, experiences large year-to-year swings in precipitation (Dettinger et al., 2011), which provided an opportunity to monitor ecohydrological dynamics across wet and dry years.

2. Methods

2.1. Site Description

The study area ("Rancho Venada"; 39.153°, −122.348°), is on a ranch 16 km west of Williams, California, USA, in the eastern foothills of the Northern California Coast Ranges (Figure 1), near the traditional territory of the Kletsel Dehe Wintun Nation. The site is affiliated with the Eel River Critical Zone Observatory, and spans elevations from approximately 150 to 350 m above sea level.

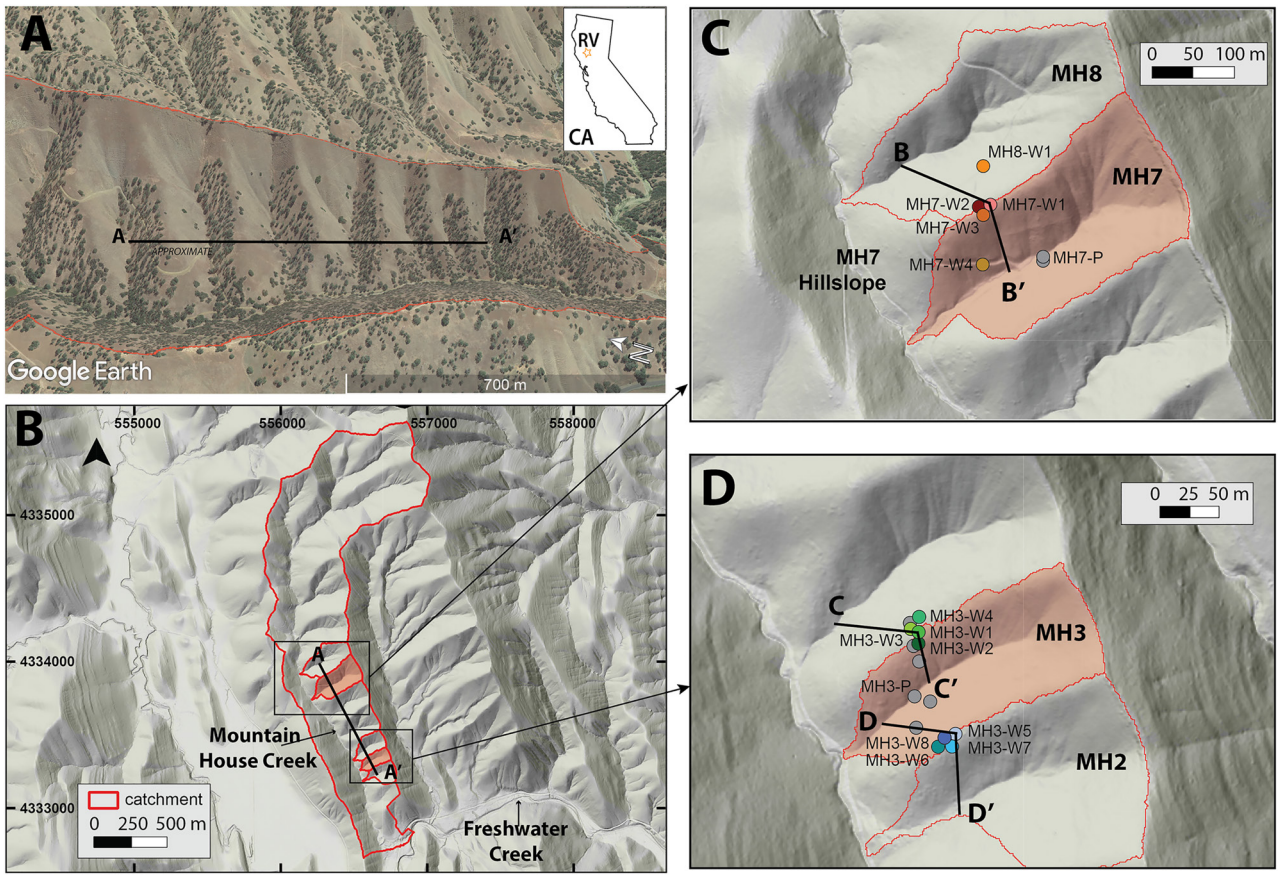

Figure 1. (a) Google Earth image of the study site (with terrain height-scaled 2×), where the red outlines delineate the Mountain House catchment and subcatchments where boreholes and monitoring infrastructure are located. (b–d) LIDAR-derived hillshade maps of the study site, with "c" and "d" zoomed in to the MH7 and MH3 hillslopes (respectively) and include borehole locations and cross-sections lines, which are used to illustrate hillslope profiles in Figure 3. Modified from Pedrazas et al. (2021).

2.1.1. Climate

The local climate is classified as hot summer Mediterranean (Csa) in the Koeppen-Geiger system (Kottek et al., 2006). The mean annual precipitation between 1981 and 2020 was 534 mm (PRISM Climate Group, 2021), the mean annual temperature was 15.8°C between 1981 and 2010 (PRISM Climate Group, 2021), and the mean annual evapotranspiration (determined from the Breathing Earth System Simulator) was 332 mm between 2001 and 2018 (Ryu et al., 2011). Snow is rare. Figure 2 shows how precipitation is strongly seasonal (concentrated in the winter months and negligible in summer), and how atmospheric demand for moisture (potential evapotranspiration) is annually much greater than—and out of phase with—precipitation. Potential evapotranspiration exceeds precipitation most of the year. Site-wide remotely sensed evapotranspiration is greatest in spring (April), months before peak energy supply in mid-summer, and exceeds precipitation throughout the summer dry season. The net positive flux of water to the atmosphere in the dry season is indicative of plant community use of stored subsurface water.

2.1.2. Vegetation

The site is a deciduous oak savanna, with an herbaceous, annual, primarily non-native groundcover, including wild oat, thistles, filaree, and California poppy. The groundcover germinates with the onset of winter rains, typically reaches peak greenness in March, and is largely dead by June. Aspect regulates the woody plant community across the study hillslopes, with negligible woody vegetation on slopes with south-facing aspects, and a community of blue oak (*Quercus douglasii*) and manzanita (genus *Arcostaphylus*, species unidentified) found on slopes with north-facing aspects. We refer to the community as a savanna because individual trees' canopies are generally not connected and the site on average has <50% canopy cover. As noted by Pedrazas et al. (2021), air

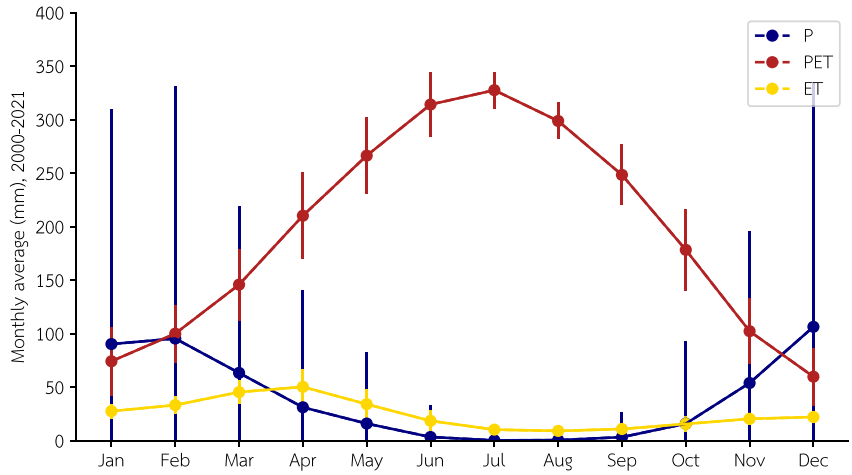

Figure 2. Composite annual timeseries of mean monthly precipitation (P), potential evapotranspiration (PET), evapotranspiration (ET) at Rancho Venada for the period 2000–2021. P is from PRISM dataset AN81d, and PET and ET are from the MODIS dataset MOD16A2. Errorbars represent one standard deviation.

photos indicate that the modern woody plant community distribution has persisted since at least 1937. The blue oaks are mature (most likely >100 years old), with very few seedlings or saplings.

2.1.3. Geology, Soils, and Weathered Bedrock

Steeply dipping (50–60° to the east) marine sedimentary beds of the Great Valley Sequence underlie the site (Rich, 1971). The bedrock is predominantly Cretaceous shale (mudstones to siltstones), with interspersed sandstone and conglomerate lenses (Pedrazas et al., 2021; Rich, 1971). The field site is characterized by regularly repeating ridge-valley topography (Figures 1 and 3), with major drainages and ridges trending parallel or perpendicular to strike. The site did not experience glaciation in the Pleistocene.

Soils at the site have been mapped as part of the Millsholm series, which are loamy, mixed, superactive, thermic lithic Haploxerepts (Soil Survey Staff, 2018). Our observations from road cuts and numerous soil pits have revealed that soils are thin (<20 cm) on south-facing slopes at the site, with patches of bare ground late in summer. In contrast, north-facing slopes have thicker soils (generally 0.5–1.5 m), with thicker groundcover. We estimate site-wide average soil thickness to be approximately 0.5 m. On both aspects, soils have abundant rock fragments, and experience plant and animal bioturbation. The landscape bears the imprint of decades of cattle grazing, with abundant contour-parallel terracettes and cross-contour walking paths.

Beneath the soil, we classify in-situ material that retains relict bedrock structure (like bedding planes) and is heavily weathered as saprolite. Saprolite grades with increasing depth into a mechanically weak, pervasively fractured layer (>50 fractures per meter; Pedrazas et al., 2021). The porosity of matrix chips (not including fracture porosity) in this layer can be nearly 20%, compared to fresh samples at greater depth which have matrix porosities of 5%–7% (Pedrazas et al., 2021). This layer extends to 6.5–7.5 m below the surface at ridgetops, and then transitions into a more discretely fractured zone, which is characterized by an increase in mechanical strength and a decrease in yellowness, indicative of less oxidation. With increasing depth, fractures become rare and isolated, separated by meters-thick layers of fresh bedrock. The weathered profile is thickest at ridgetops, and thins toward the channels, where fresh bedrock can be found within centimeters of the surface (Huang et al., 2021; Pedrazas et al., 2021). Figure 3 depicts the subsurface weathering profile in cross-section view across the largest study hillslope.

2.2. Precipitation, Temperature, and Vapor Pressure Deficit Observations

2.2.1. Local Monitoring

A tipping bucket rain gauge (model TB4) was installed on February 18, 2017 on a relatively wind-sheltered, tree-free flat at the mouth of the Mountain House catchment (39.142323°, −122.343214°), 500 m south of the MH3

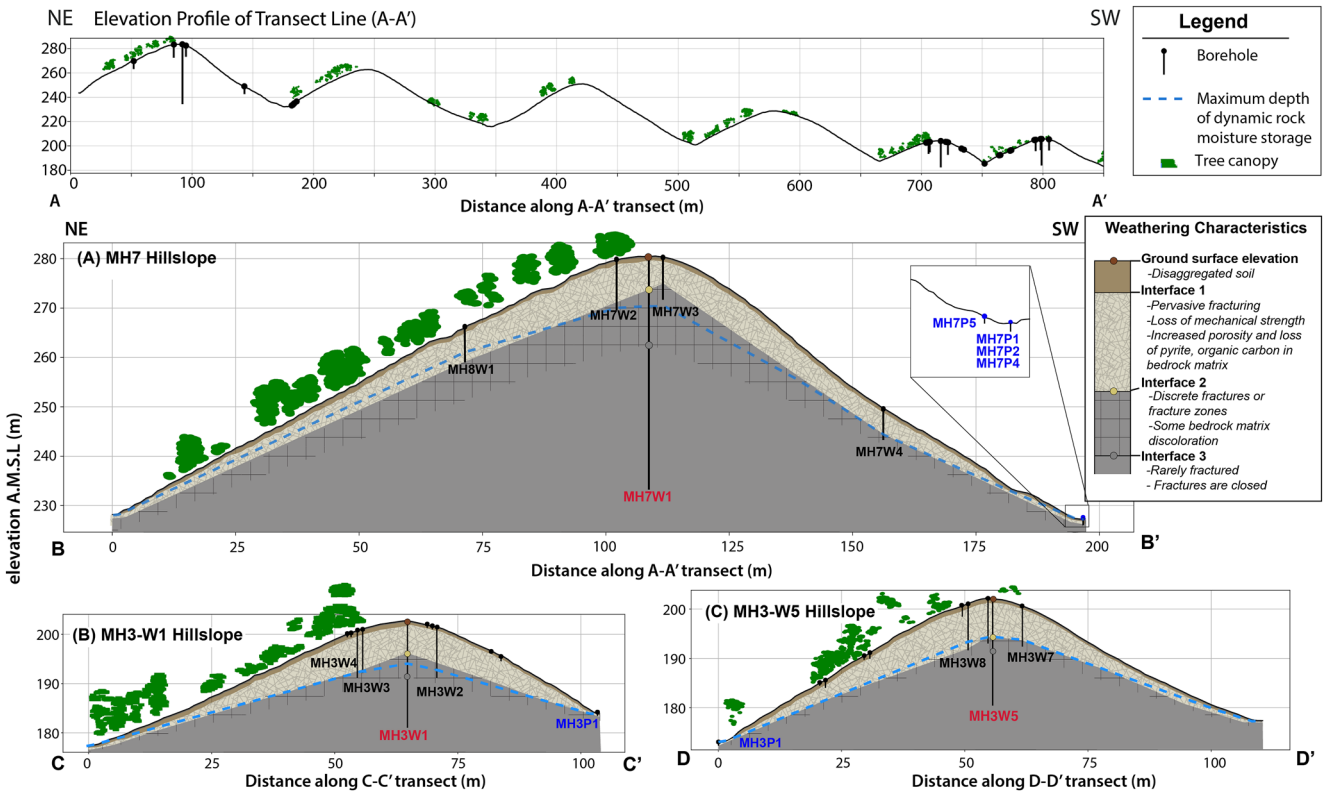

Figure 3. Elevation profiles, borehole locations, and subsurface weathering characterization of hillslopes shown in Figure 1. Tree canopy and surface topography are derived from LiDAR. Hatching showing zone of discrete fractures is meant to delineate the depth extents and not actual strike/dip of fractures. Fractures are typically either high angle (60–80° dip) oriented at a strike of approximately 97° or low angle (30–40° dip) fractures oriented at a strike of approximately 172° (right-hand rule convention (Pedrazas et al., 2021). Figure modified from Pedrazas et al. (2021).

study catchment. A second TB4 tipping gauge was later installed on the ridge above the MH7 monitoring wells on March 24, 2019. Over their overlapping time period, the ridge-top gauge recorded 95% of the precipitation of the gauge at the mouth, which could be explained by wind-induced undercatch at the ridge-top location. We use the catchment-mouth gauge to evaluate precipitation inputs in relation to rock moisture dynamics over the monitoring period, and assume that it is representative of rainfall over the relatively small study area (0.5 km^2).

Local vapor pressure deficit (VPD), the difference between saturated and actual vapor pressure, was determined from relative humidity and temperature measurements made at the ridgetop weather station with a Vaisala HMP60 probe, following Snyder (2005).

2.2.2. Historical Climate

To contextualize our monitoring period within historic precipitation and temperature variability at the site, we rely on PRISM climate datasets (AN81d). These data are available for the past four decades (1982–2021 water years) at daily resolution (PRISM Climate Group, 2021), and were queried via the Python API from the Google Earth Engine. The historical data are presented to show relative long-term inter-annual variability rather than locally accurate values; compared to our local gauge, we found that the PRISM precipitation data can overestimate the locally recorded precipitation by up to 17% (in the 2020 water year, e.g.,).

2.3. Remotely Sensed Enhanced Vegetation Index (EVI), Evapotranspiration (ET), and Potential Evapotranspiration (PET)

EVI, a proxy for plant greenness, productivity, and evapotranspiration (Huete et al., 2002), was obtained from the MODIS MCD43A4_006_EVI dataset from the Google Earth Engine (Gorelick et al., 2017). The pixel size is approximately 500 m and the dataset represents a 16-day composite of Terra and Aqua data. A 7 day rolling median resample was also performed before averaging across years (see analysis script linked in the Data

Availability Statement for complete data acquisition and processing steps). ET and PET were obtained from the MODIS dataset MOD16A2, and were extracted with a 1 km buffer centered on 39.153610°, −122.343737°.

2.4. Oak Sapflow Velocity

Heat pulse velocity sapflow probes (model: SF3, manufacturer: Edaphic Scientific; Forster 2019) capable of measuring forward and reverse flow were installed at breast height on four mature blue oak trees on April 28, 2019. The trees are situated between 10 and 20 m from the MH7 ridgetop on the north-facing slope, adjacent to the weather station. Measurements were taken every half hour, and for presentation and analysis purposes outliers were excluded, and the timeseries were normalized by the maximum and minimum recorded for each tree, then averaged across all sensors and normalized again. This produces a timeseries that shows relative changes in sapflow through time, rather than absolute transpiration rates, which would require (presently unknown) information about sapwood thickness. One sapflow sensor failed in spring 2021 and was not replaced, and a datalogger failure occurred between August 29, 2021 and October 13, 2021. Data missing in this time were filled via linear interpolation. Sensors were not moved over the course of the study to minimize sensor damage. This could potentially lead to artifactual sapflow readings if tree wound response altered sapflow near the probes. No significant wound response was visible over the course of the study, and evidence from sapflow observations in the closely related deciduous oak *Quercus garryana* indicate that measured sapflow velocities return to similar values under equivalent environmental conditions across multiple seasons without sensor replacement (Hahm et al., 2018).

2.5. Water Potential

Water potentials were measured with a Scholander-type pressure chamber (Scholander et al., 1965; PMS Instruments Model 1000) on razor-excised shoots accessible from ground height from mature, randomly selected blue oak and manzanita located in upslope positions near the monitoring wells, following the methodology described in Hahm et al. (2020). Measurements were made within 2 h before dawn (pre-dawn). Two shoots from each tree and 4–8 trees of each species were typically measured at each sampling time. Occasional measurements lacked sufficient nitrogen tank gas pressure to balance the shoot pressure. These measurements should be therefore considered lower bound estimates of the absolute magnitude of water potential, and are noted via arrows in display. Measurements were grouped by species at each sampling time, then averaged by tree and across all individuals. The water potential measurement campaigns were unfortunately episodic in nature, and data are missing in 2019.

2.6. Monitoring Boreholes

Three hillslopes and their adjacent channels were selected for subsurface hydrologic monitoring. Here, we briefly describe the network of monitoring boreholes at these locations (see map in Figure 1 and borehole cross-sections in Figure 3); complete descriptions of drilling and completion methods are available in the supplementary information of Pedrazas et al. (2021).

A deep borehole was drilled at the ridgetop of each study hillslope to the depth of the adjacent channel. Because the space between the borehole wall and the outside of the PVC casing was filled with cement in the upper 10 m these three boreholes are used only to describe weathering patterns and deep groundwater level dynamics, not vadose zone moisture dynamics. These deep boreholes (MH7W1, MH3W1, MH3W5) were drilled via a track-mounted rig with a combination of standard-penetration test hammering and water-cooled diamond core bit, and cased with continuously slotted PVC below a depth of 9.1 m (MH7W1) and 6.1 m (MH3W1, MH3W5) to their maximum depths of 47.6, 21.5 and 21.6 m, for MH7W1, MH3W1, and MH3W5, respectively.

Ten boreholes located on mid-slope to ridge-top positions are used to monitor bedrock vadose zone moisture dynamics to maximum depths ranging between 6.3 and 10.7 m (holes MH3W2, MH3W3, MH3W4, MH3W6, MH3W7, MH3W8, MH7W2, MH7W3, MH7W4, and MH8W1). These boreholes were drilled via flight auger and have diameters between 6.4 and 8.9 cm, and are cased with variable lengths of solid 5 cm diameter PVC near the surface (to minimize the potential for downward drainage within the borehole from surface water) followed by continuously slotted 5 cm diameter PVC to the bottom of the borehole.

To explore near-surface saturated zone dynamics and pressure head gradients, numerous shallow piezometers were installed across the site (boreholes with the letter "P" in their name refer to piezometers). Boreholes for these piezometers were augered (on the hillslopes) or core-drilled (in/by the channels), and cased with solid PVC that was slotted at its base (typically the lowest 5–10 cm), back-filled with sand around the slotted region, and then back-filled with bentonite and native material.

2.7. Soil Moisture

The enhanced NASA-USDA remotely sensed soil moisture product uses the Soil Moisture Active Passive (SMAP) satellite to map near-surface soil moisture at 10 km pixel resolution. Here, as a proxy for relative near-surface soil moisture content, we report the normalized range (i.e., rescaled from 0 to 1) of the surface soil moisture reservoir. We emphasize that this metric is not necessarily an accurate representation of actual soil moisture content for our site, given the shallow effective sensing depth of the SMAP program (top 5 cm only; Entekhabi et al., 2010) and the large pixel sizes which average over the significant north-south slope heterogeneity in our field area. However, in the absence of in situ soil moisture observations this product does serve as a potentially useful relative metric of surface dryness. These data were queried from the Google Earth Engine (NASA_USDA/HSL/SMAP10 KM_soil_moisture image collection; Sazib et al., 2018).

2.8. Bedrock Vadose Zone Moisture Dynamics

Bedrock vadose zone moisture dynamics were monitored via down-borehole neutron probe surveys (Long & French, 1967). Data are reported here for the medium-depth, augered boreholes. Pedrazas et al. (2021) first reported on the observed depth of dynamic water storage by contrasting a single pair of wet and dry season observations, following methodology and using instrumentation similar to Salve et al. (2012), Schmidt and Rempe (2020), Rempe and Dietrich (2018), and Hahm et al. (2020). Here, we report observations at roughly monthly intervals from early 2019 through the 2021 water year. Surveys were made with models 501DR and 503DR Hydroprobes (CPN) starting approximately 0.5 m below the ground surface and progressing downwards in 30.5 cm vertical intervals within the unsaturated zone, stopping immediately above the groundwater level (if present) at the time of survey or bottom of the borehole. At each interval, neutron counts were recorded for 25–30 s, and converted to volumetric water content following our probe- and borehole diameter-specific calibration equations originally provided in Rempe and Dietrich (2018). Because each probe differs in standard counts, we inter-calibrated probes to the original probe used in developing the volumetric moisture content conversion equations by linearly regressing counts collected with each probe across borehole depths which exhibit no temporal variation.

In addition to reporting vertical moisture profiles, we quantified depth-integrated temporal changes in rock moisture content (below the local soil depth) at each borehole. Following the approach in Hahm et al. (2020), each measurement survey is differenced with the volumetric water content of the driest-recorded survey, resulting in a relative change in moisture content. This difference in water content is multiplied by the vertical measurement interval (305 mm) and summed across the vertical profile to quantify the dynamic change of unsaturated water volume in the weathered bedrock per unit surface area.

Standard counts and visual analysis of data were used to assess probes for malfunction, leading to the exclusion of surveys of individual boreholes across the study period. Instrument precision (0.31% volumetric water content) is estimated via the standard deviation of repeat measurements taken at a particular depth for each survey (Hahm et al., 2020). The average estimated uncertainty in reported integrated dynamic storage values is approximately ±5% (Hahm et al., 2020; Rempe & Dietrich, 2018).

2.9. Groundwater and Stream Stage Dynamics

Pressure transducers (Solinst Leveloggers) were used to record water level dynamics starting in November 2018, to the present in MH3W1, MH3W5, and MH7W (deep ridgetop boreholes), MH3P1, MH7P1, MH7P2, MH7P3, MH7P4, MH7P5 (near- or in-channel piezometers), and April 2019 to the present in MH3W2, MH3W3, MH3W4, MH3W6, MH3W7, and MH3W8 (medium-depth upper hillslope boreholes), and from December 2019 to present in the MH3GAGE and MH7GAGE stilling wells (located at sub-catchment channel outlets; see Figure 1 for

locations). Transducers were also placed in six mid-to-upper hillslope position piezometers (MH3P10, MH3P11, MH3P12, MH3P16, MH3P17, MH3P18) in November 2018 but removed for use elsewhere in March 2019 after no water level dynamic was detected during that very wet period.

When plotting continuous timeseries, we corrected for periods when the transducers were removed for data downloading and other short anomalies due to sensor malfunction or other unknown causes by applying a rolling median filter with a 12 hr window to the timeseries. This resulted in smoothed hydrographs, but did not result in the elimination of any major features or missing events. Step-offsets arising from pressure transducers being replaced to different depths after removal and replacement for data downloading were manually corrected.

The offline, battery powered transducers are accurate to ±5 mm, collect data at 15 min intervals, and are atmospheric-pressure compensated with two barometers (one on the weather station barometer and another in the MH3 valley bottom). Approximately monthly manual e-line measurements of water levels were used to validate the pressure transducer observations and determine borehole-specific atmospheric pressure offset corrections.

2.10. Woody Plant Mapping

We mapped all woody plants with diameter at breast height (DBH) > 5 cm in a 1.5 ha area spanning ridge-top to channel bottom, centered on the MH8W1 monitoring borehole (see Figure 3 for location). DBH and species information were recorded on October 19, 2019 using the FieldMove Clino app on an iPhone X, which also recorded location via the internal GPS receiver.

3. Results

3.1. Meteorological Observations

During the study period, the site experienced a wet year followed by two extreme drought years. Figure 4a shows that in the first water year of monitoring (2019), the cumulative precipitation was 30% larger than average. The 2019 wet season was also notable for high intensity rain events in February that triggered numerous shallow landslides across the site (Sanders et al., 2019). There were also large storms relatively late in the wet season (mid-late May). Each of the subsequent two wet seasons (in the 2020 and 2021 water years) experienced less than half the average precipitation and were in the lowest fifth percentile of recorded rainfall totals over the last four decades. February 2020, saw an extended dry spell that occurred across Northern California; for the first time in recorded history no rain fell on nearby Sacramento that month. The 2021 water year was the driest in the preceding four decades.

The 2020 and 2021 water years were not only anomalously dry, but also anomalously hot. Figure 4b shows both water years having frequent summer heat waves. 2021 was also particularly warm over the course of the wet season, and overall that water year was the second warmest in the preceding four decades.

Based on the US Drought Monitor, the site had a drought intensity of D0 (Abnormally Dry) in January 2020, and progressed through D1 (Moderate Drought), D2 (Severe Drought), and reached D3 (Extreme Drought) at the end of the 2020 water year. The site reached the highest possible drought intensity of D4 (Exceptional Drought) in late May 2021, which was sustained through the 2021 dry season (https://droughtmonitor.unl.edu/).

3.2. Woody Plant Composition

The woody plant survey revealed that blue oak was the dominant tree species, with 6.44 m^2ha^{-1} basal area at breast height and 145 individuals >5 cm DBH ha^{-1}, compared to 0.44 m^2ha^{-1} and 13 individuals >5 cm DBH ha^{-1} for manzanita. The blue oak DBH was 22.0 ± 8.9 cm (mean ± 1 s.d.), and the manzanita DBH was 18.9 ± 8.1 cm, for all individuals with DBH >5 cm.

3.3. Rooting Observations

During drilling, the deepest roots were observed at 6–8 m in the MH3W5 borehole, and 5–6 m at the MH7W2 borehole. Figure 5a shows a photo of two small woody roots emerging from a cored sample of bedrock. Road-cuts revealed pervasive rooting in fractured bedrock up to 3 m below the surface near the base of the hillslopes

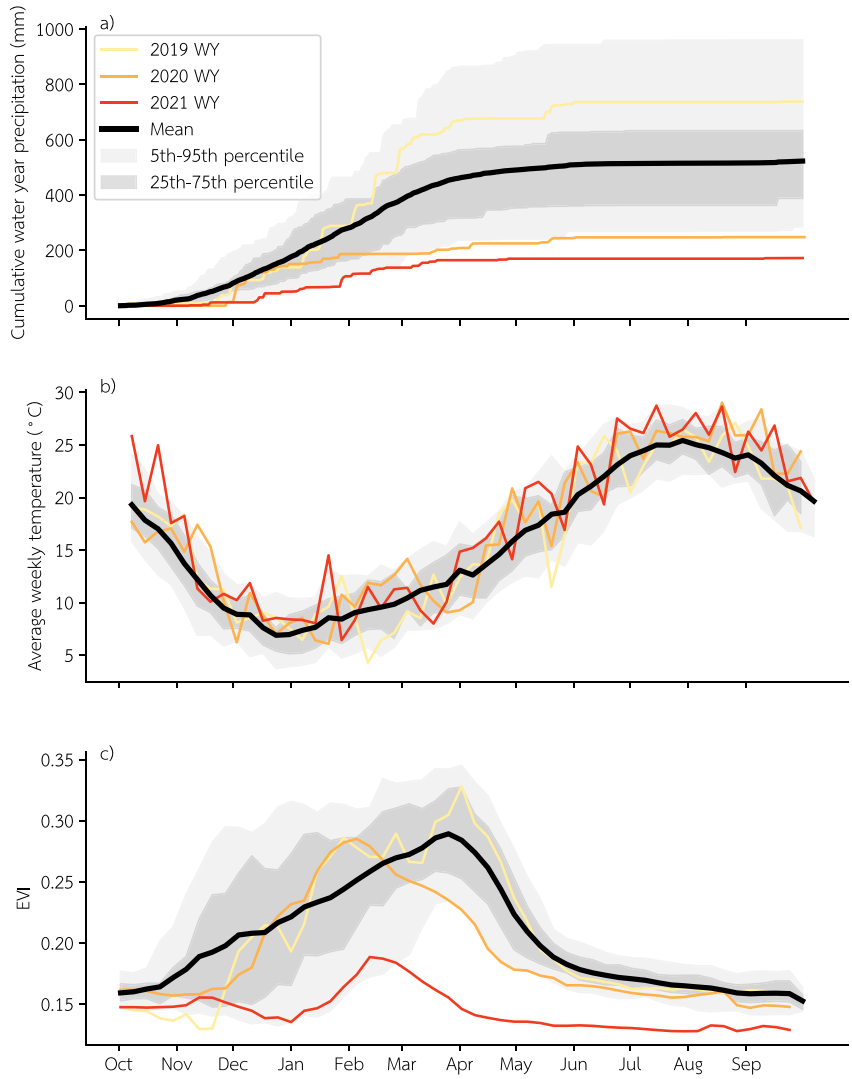

Figure 4. (a) Cumulative precipitation patterns at Rancho Venada for the 1982–2021 water years (WY), from the PRISM AN81d dataset. (b) Average weekly temperature from the PRISM AN81d dataset over the same time period. (c) Enhanced Vegetation Index (EVI) for the 2001–2021 water years from the MODIS MCD43A4_006_EVI dataset. In each subplot, the three study years highlighted as individual colored lines are also included in the statistical summaries.

(Figures 5b and 5c). Blue oaks at the site were observed to be rooted directly into bedrock where soil cover is absent (Figure 5d). Woody roots were also observed to extend significant distances laterally. Landslide scars across the site that exposed the soil and weathered bedrock profile revealed that thick (>3 cm diameter) roots can be at least 14 m from the nearest tree trunk (a distance of more than two canopy radii).

3.4. Site-Wide Greenness Dynamics

Figure 4c shows the distribution of annual site-wide EVI, a proxy for plant greenness, productivity and transpiration. On average, EVI increases steadily from the start of the wet season in October to its peak in early April, which typically coincides with the start of the dry season. EVI then drops rapidly for a 2-month period, until June, when a slower rate of decline prevails until the end of the dry season. Interannual variation in EVI is large in the wet season, with wider 25–75th and 5–95th percentile bands in the winter compared to summer.

Figure 4c also highlights (as individual colored lines) the three monitored water years. Rain in the relatively wet 2019 water year didn't arrive until later in November, which triggered a later-than-average greenness increase. Following heavy mid-winter rains, the peak greenness in April was higher than normal. The first monitored

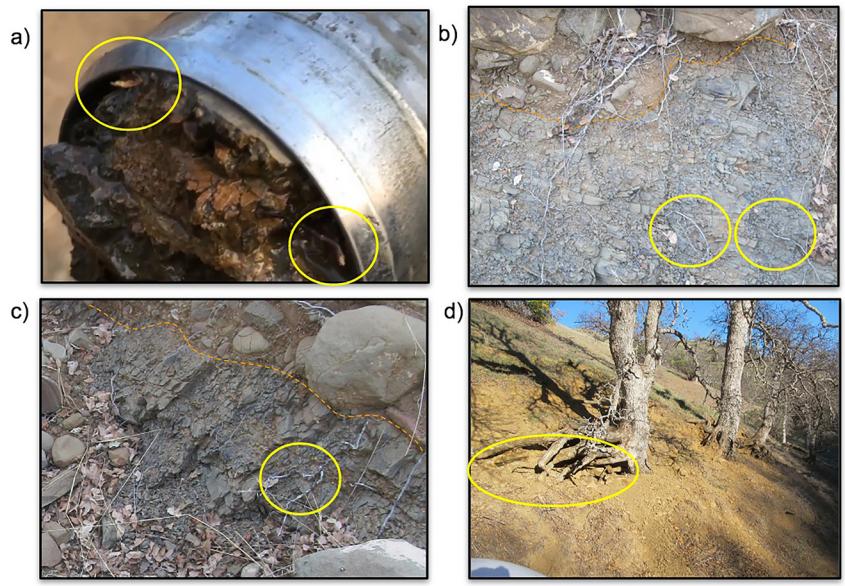

Figure 5. Yellow circles highlight roots in fractured bedrock. (a) Roots in bedrock core sample from 7 m depth in borehole MH3W5. (b and c) From road cuts; orange dashed line denotes contact between in situ, weathered bedrock (below) and mobile alluvium/colluvium (above). (d) Mature blue oaks rooted directly into weathered bedrock. Highlighted roots are approximately 1 mm, 1 cm, 2 cm, and 15 cm diameter in a, b, c, and d, respectively.

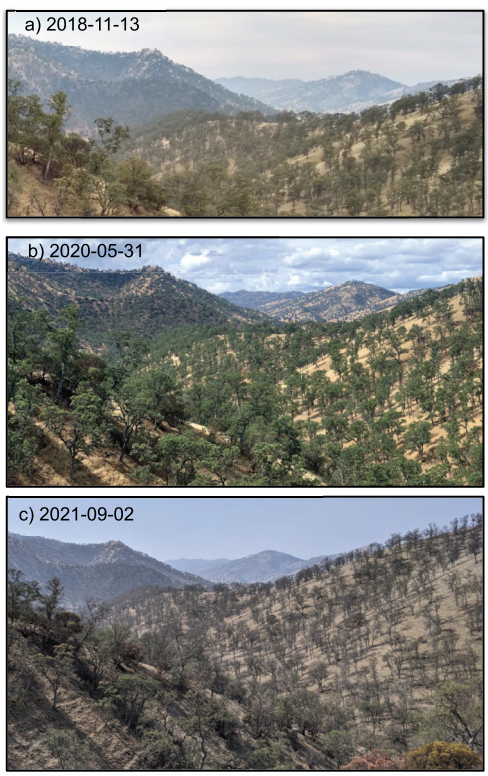

Figure 6. Photos taken before, at the start of, and during the extreme drought (a, b, and c, respectively) highlight changes in woody plant community canopy cover, with (c) showing widespread canopy loss after two dry years at a time of year when the woody plant community is normally fully leafed out. Perspective is from the MH3 hillslope looking south.

drought water year (2020) is notable for rains concentrated in the early part of the wet season, and peak greenness 2 months earlier than average. The subsequent very dry and warm water year (2021) was near the fifth lowest percentile of EVI for the first part of the wet season. Peak greenness preceded the average by 1.5 months, and only reached a magnitude typically seen in June, when the herbaceous annual groundcover has largely senesced. The subsequent 2021 dry season trajectory is lower than any observed during the MODIS monitoring program.

Monthly field visits indicated that the remotely sensed EVI signal is primarily controlled by the growth and senescence of the herbaceous annual groundcover, which by area constitutes the majority of the MODIS pixel footprint. Blue oak at the site lost their leaves sometime after late November 2018 and in early December 2019, for example, exerting a minor influence on the EVI signal. In contrast, peak EVI tended to coincide with visual assessments of peak herbaceous groundcover greenness, and winter growth and spring senescence coincided with positive and negative EVI slopes, respectively. The herbaceous annual groundcover is not uniform, however: the satellite pixels integrate distinct aspect-governed greenness trajectories. In late February 2020, for example, north-facing slopes were still green while south-facing slopes were brown. The site-wide EVI signal integrates this spatial heterogeneity, along with the (apparently minor) impact of the winter deciduous blue oak leaf out and leaf loss. The dynamics and limitations of remotely sensed phenology in heterogeneous blue oak savannas are extensively discussed by Liu et al. (2017).

3.4.1. Branch and Canopy Dieback

We observed blue oak at the site in non-drought conditions keeping their leaves until the first rains, which sometimes arrive very late in the year. Figure 6a shows how the woody plant canopy is still largely intact in November 2018. Figure 6b shows a healthy woody plant canopy at the start of the

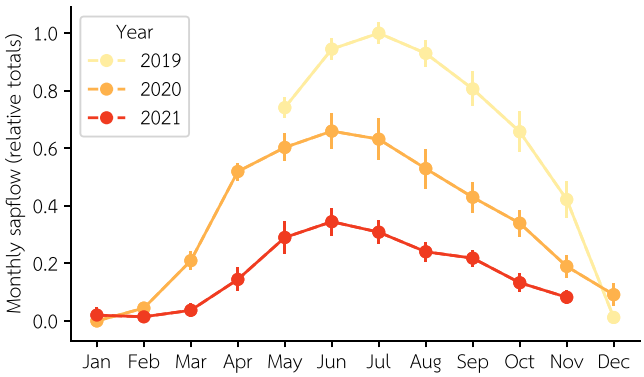

Figure 7. Relative monthly sapflow totals, averaged across normalized timeseries from four monitored blue oaks. Error bars represent one standard deviation.

first drought in the dry season in May 2020, and Figure 6c shows the extreme reduction in woody leaf area in the second summer of drought: the oaks had significantly reduced individual leaf sizes and fewer leaves, with desiccated distal branches that snapped easily, and the manzanita exhibited signs of branch dieback (red-brown leaves). It remained unclear at the conclusion of the study (September 2021) whether individual woody plants across the site were experiencing a widespread mortality event.

3.5. Oak Sapflow

Figure 7 shows relative monthly sapflow totals, averaged across the four monitored blue oaks. The sapflow timeseries is a proxy for oak transpiration, and is similar in shape and timing to the PET timeseries (Figure 2). The oak sapflow timeseries is more symmetrical than site-wide greenness (Figure 4c), which tends to rise slowly and has a rapid recession in the spring. Trends in oak sapflow lag site-wide greenness by at least 3 months. Oak water use was lower in years with less winter precipitation: dry season oak sapflow in 2019, following a relatively wet winter, was roughly twice as high as in 2020, following the first drought year, and thrice as high as in 2021, following the second drought year (Figure 7). Across all monitored years, peak sapflow occurred in June-July, coincident with peak solar energy inputs. Non-zero sapflow in winter when the oaks lacked leaves (e.g., February) is likely attributable to tissue refilling, evergreen mistletoe, and/or stem water loss.

Figure 8 compares daily total oak sapflow as a function of atmospheric dryness or water demand, quantified as the vapor pressure deficit (VPD). Variations in sapflow for a particular VPD correspond to changes in leaf phenology and subsurface water availability. For example, in 2020, low values of sapflow at 2 kPa VPD occur during the early dry season before full leaf-out. High sapflow values at 2 kPa VPD occur during mid-summer when the trees are fully leafed out. Medium sapflow values at 2 kPa VPD occur in the late dry season when the leaves are still fully leafed out, but subsurface water availability is diminished. Between years, large differences in sapflow for a particular VPD and day of year correspond to differences in preceding wet season rainfall totals, which as will be described below, also drive differences in subsurface water storage. For example, in 2019, after a relatively wet winter, oak water use for a particular atmospheric water demand was more than twice as high as in 2020 and 2021, the two drought years.

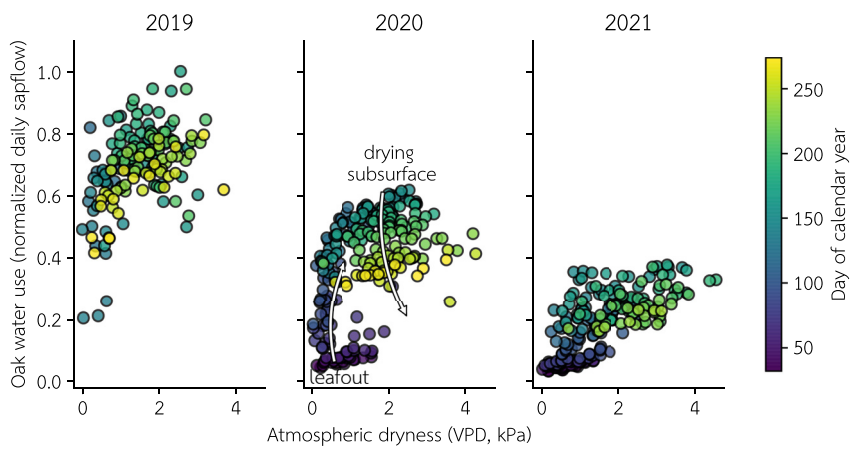

Figure 8. Oak sapflow across years as a function of vapor pressure deficit. Each point represents total (relative) daily sapflow from February-September. Arrows and annotation in 2020 show interpreted controls on differences in sapflow for a given atmospheric water demand.

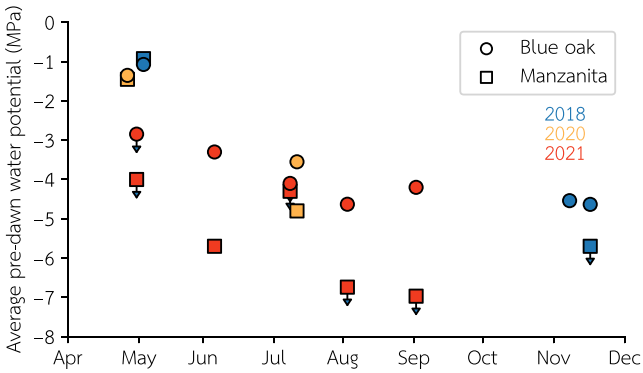

Figure 9. Site-wide average pre-dawn shoot water potential (a proxy for root zone water availability), as a function of time of year, categorized by calendar year (color) and species (symbol). Small vertical arrows below symbol denotes inclusion of measurements which lacked sufficient nitrogen gas pressure to balance shoot pressure, and therefore the true water potential is lower than displayed.

3.6. Water Potential Dynamics

In 2018 (which ranged between D0–D1 abnormally dry to moderate drought) and 2020, pre-dawn water potential, a metric of subsurface water availability, was relatively high (closer to zero) after leaf-out in April, and decreased through the dry season, reaching very low values (−4.5 MPa for oaks and −5.5 MPa for manzanitas) before leaf abscission (Figure 9). Early in the dry season, oaks and manzanitas had similar pre-dawn water potentials, but manzanitas tended to have lower water potentials than oaks on contemporaneous sampling dates in mid-summer to fall. Although data were not collected in the relatively wet year of 2019, water potentials were much lower in the second year of drought (2021) than in the first (2020) for oaks at comparable times of year, indicative of lower rhizosphere water availability. Notably, by the end of April 2021 oak pre-dawn water potentials were already nearly −3 MPa. By June 2021 manzanita pre-dawn water potentials neared −6 MPa.

The lowest overall water potential values were measured in September 2021, with several individual manzanita samples being insufficient to measure at the available gas pressure of 7 MPa.

3.7. Rock Moisture Dynamics

3.7.1. Relationship to Precipitation

Variable inter-annual precipitation resulted in distinct wet-up dynamics in the soil and weathered bedrock unsaturated zones (soil and rock moisture, respectively). Figure 10 shows how total wet season precipitation declined drastically from the relatively wet 2019 WY through 2 years of increasingly extreme drought (2020 WY and 2021

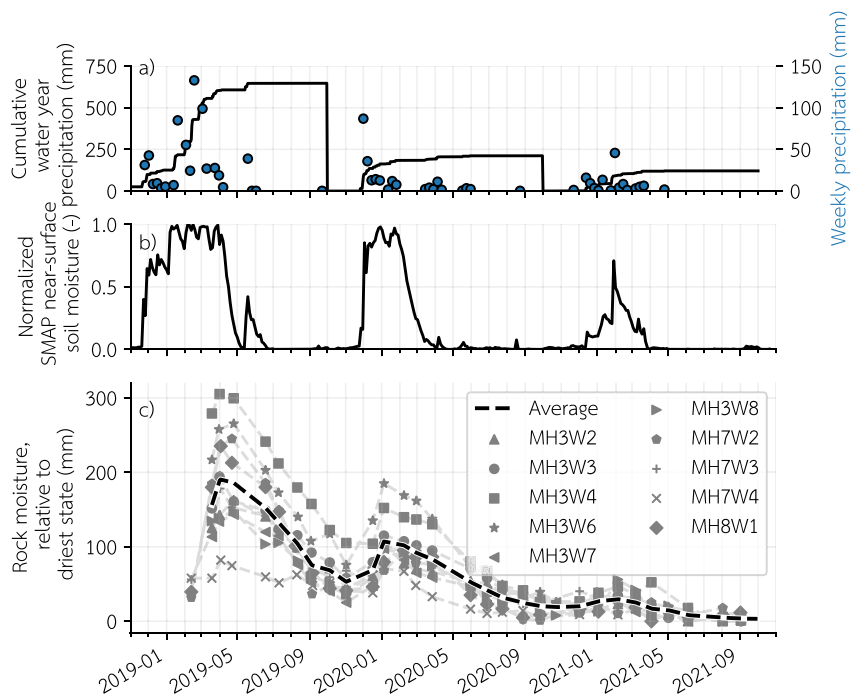

Figure 10. (a) Cumulative water year and weekly precipitation timeseries, from the local precipitation gauge located at the MH catchment mouth. (b) Remotely sensed (SMAP) near-surface normalized soil moisture timeseries. (c) Overall site average (black) and individual borehole (gray) neutron probe-inferred weathered bedrock vadose zone water content (i.e., rock moisture) timeseries. Each individual borehole's water content is plotted relative to its driest state, defined as 0 mm rock moisture content. Dashed lines are linear interpolations between the roughly monthly spaced surveys, denoted with points. See map and cross-section in Figures 1 and 3 for borehole locations.

Table 1
Annual Precipitation, Maximum Dynamic Rock Moisture Gains and Losses Over Specified Time Periods, and Inferred Per-Tree Average Daily Use of Rock Moisture

Water year	Total precipitation (mm)	Oct-May max. rock moisture gain (mm)	Jan-Sep max. rock moisture loss (mm)	Jun-Sep max. rock moisture loss (mm)	Jun-Sep avg. per tree daily rock moisture use (L)
2019	646.7	–	120.8	93.3	53.7
2020	211.6	54.1	87.0	32.3	18.6
2021	120.9	20.4	26.4	5.6	3.2

Note. No Oct-May maximum rock moisture gain is available in the 2019 WY due to the unknown extent to which drilling boreholes resulted in artifactual moisture content at the start of the wet season.

WY). Relative near-surface soil moisture (inferred from the remotely sensed SMAP satellite mission) reached the same maximum in the 2019 WY and 2020 WY, but reached a lower maximum in the 2021 WY. In winters in which a maximum soil moisture content is reached, the combined observations of low ET rates, sustained rainfall and lack of surface hillslope runoff locally imply that the soil rapidly passes water to the underlying unsaturated weathered bedrock. In all three dry seasons, near-surface soil moisture declined rapidly and remained at a low, constant value for the duration of the summer dry season. In contrast to near surface soil moisture, the neutron probe surveys indicated the maximum wet season rock moisture content varied as a function of precipitation across all 3 years. In the wet 2019 WY, which had 646.7 mm of locally recorded precipitation, the maximum site-wide average dynamic rock moisture (i.e., relative to its driest state) was ≈190 mm. That year rock moisture did not increase with additional rains after March, indicative of having reached storage capacity. Subsequent rains triggered relatively rapid downward drainage of water to the saturated zone. Rock moisture content expressed as its value relative to the minimum attained over the observation period in individual boreholes ranged from more than 300 mm (for MH3W4, which is situated near trees) to just under 100 mm (for MH7W4 which has no nearby woody vegetation). In the first drought year (2020 WY), 211.6 mm of total precipitation was insufficient to bring rock moisture to its previously observed maximum value. In the second, extremely dry drought 2021 water year (just 120.9 mm total precipitation), rock moisture was similarly not replenished to the previous years' maximum observed values. The lowest observed site-wide average summer dry season dynamic rock moisture content decreased each year. Thus, although the total amount of dry season rock moisture drawdown in the drought years was smaller, the weathered bedrock unsaturated zone was drawn down to a progressively drier absolute state.

Table 1 summarizes the maximum dynamic rock moisture gains and losses between specified time periods across water years in relation to precipitation (i.e., the patterns present in the bold dashed line in Figure 10c). The intra-seasonal relative gains in rock moisture are smaller than the maximum overall values reported for the 2020 and 2021 water years because the subsurface was not at its driest state at the start of either of these seasons. We cannot calculate the intra-annual gain for the 2019 WY because the first neutron probe surveys occurred after the start of the rains. In the 2019 WY, approximately the same amount of rock moisture was lost between January and September as the total amount of precipitation in the 2021 WY. Table 1 separately highlights the maximum intra-annual loss between January and September and June and September. The first time period includes wet winter months and spring months, so it can potentially include downward drainage to groundwater and herbaceous groundcover evapotranspiration. In contrast, between June and September, no groundwater recharge is likely, the herbaceous groundcover is senesced, and therefore rock moisture depletion is primarily attributable to woody vegetation. Abiotic evaporative fluxes from the weathered bedrock vadose zone could also play a role, but we suspect they are minimal based on the nearly static rock moisture dynamic in borehole MH7W4 (which is in an area without trees) in the latter portion of the dry season, in contrast to continued declines in rock moisture in the other boreholes near trees (Figure 10c). In each drought water year (2020 and 2021), the maximum amount of rock moisture lost was greater than that gained when considered over the January-September timeframe, but not the June-September timeframe.

Table 1 additionally reports the average amount of water drawn from the weathered bedrock vadose zone per mature tree from June to September each year. This estimate comes from multiplying the inverse of the trees per hectare (Section 2.10) by the decline in rock moisture, under the assumption that the entire rock moisture decline over that time period is attributable to tree transpiration. In 2019, each tree used on average 6.4 m^3 of bedrock vadose zone water from June to September, or 53.7 L per day; by 2021, that quantity had been reduced by more than a factor of ten.

The time lag between incoming rainfall and SMAP-inferred soil moisture increase is on the order of days, whereas the increase in rock moisture content (within our ability to detect changes given our measurement frequency) appears to be on the order of days to weeks. Figure 11 shows rock moisture depth profiles at roughly monthly intervals for borehole MH8W1, which is situated among a stand of blue oaks on a north-facing hillslope. In this

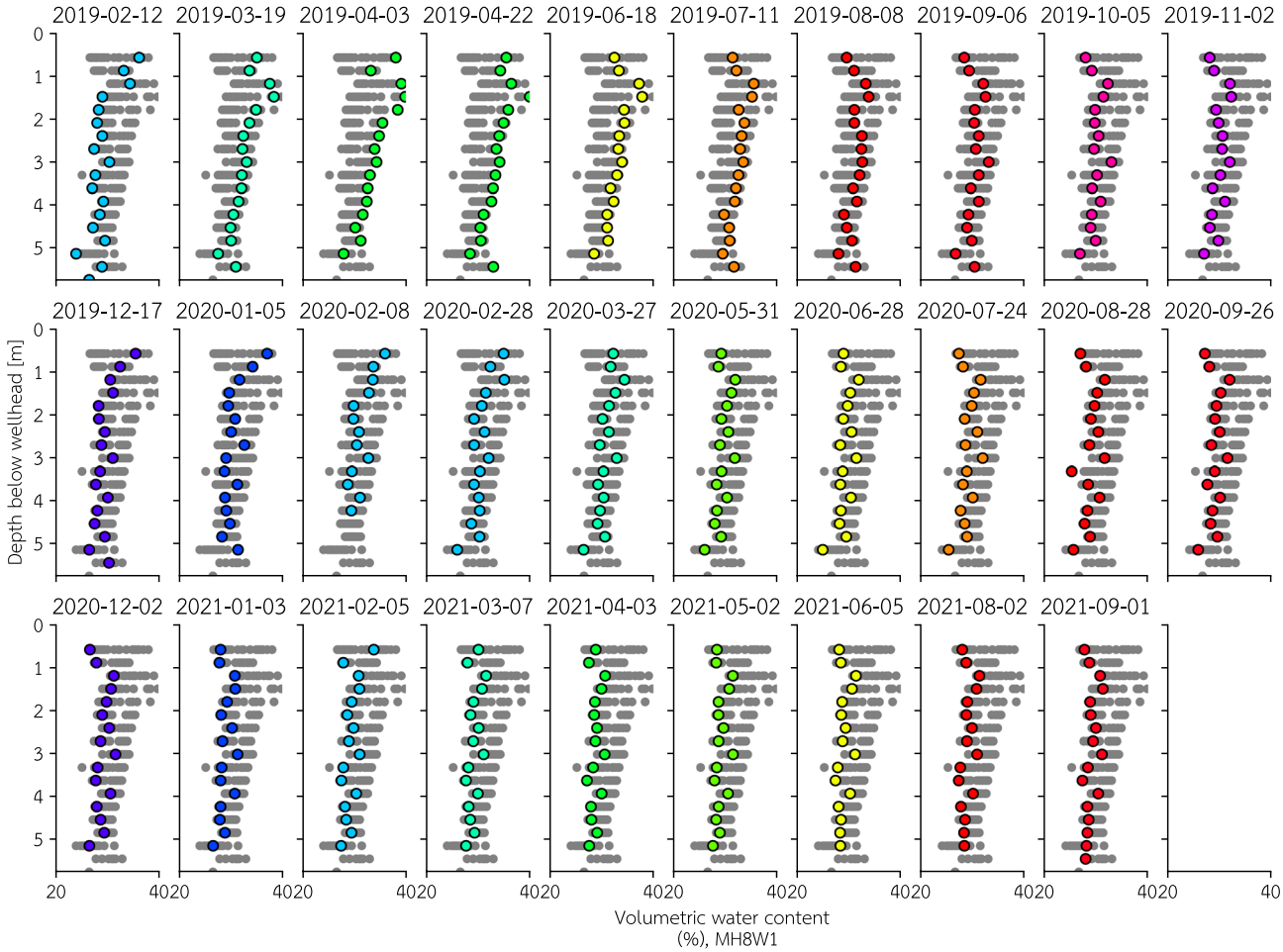

Figure 11. Depth profiles of rock moisture content through time for borehole MH8W1. Colored points in foreground represent the volumetric water content (theta) at the time of survey (color corresponds to time of year across all plots), and gray points in background show the range of all data ever collected. For corresponding plots for all boreholes, see Supplementary materials.

figure (and similar figures for the other boreholes, available in the supplementary computational notebooks), horizontal movement between dates of the colored points in the foreground indicates gains (rightward) or losses (leftward) of moisture content. Several hydrologic phenomena of interest are visible in the depth profiles: (i) wetting fronts within the weathered bedrock vadose zone appear each wet season, with early increases in moisture content occurring in the uppermost part of the profile; (ii) seasonal rock moisture dynamics can be relatively large to depths well below the soil (>5 m below the ground surface); and (iii) the primary location of dynamic rock moisture (change in water content) varies across water years. For example, in January of the 2020 WY, the top meter of the profile reached the same peak wetness state as the 2019 WY, while the lower portion of the profile remained drier. In the 2020 WY, most rain arrived in a sequence of storms early in the wet season (Figure 10), and the wetting front stalled after these early storms. In the 2021 WY wet season, only the very top portion of the profile gained moisture, and only to a small extent relative to prior years.

3.7.2. Relationship to Transpiration

Figure 12 compares daily values of oak sapflow, VPD, and rock moisture content. Oak sapflow is better correlated with rock moisture content than VPD, and for a given VPD, oak sapflow tends to be higher when rock moisture content is higher. We quantified the extent to which variance in oak sapflow could be explained by atmospheric water demand (expressed as VPD) and rock moisture availability (from the cross-site daily interpolated values) across all study years during the months of June, July, and August, via ordinary least squares regression (full analysis details are available in a computational notebook in the data repository linked in the Data Availability Statement). When considered individually, a fit to VPD alone explained a negligible amount of

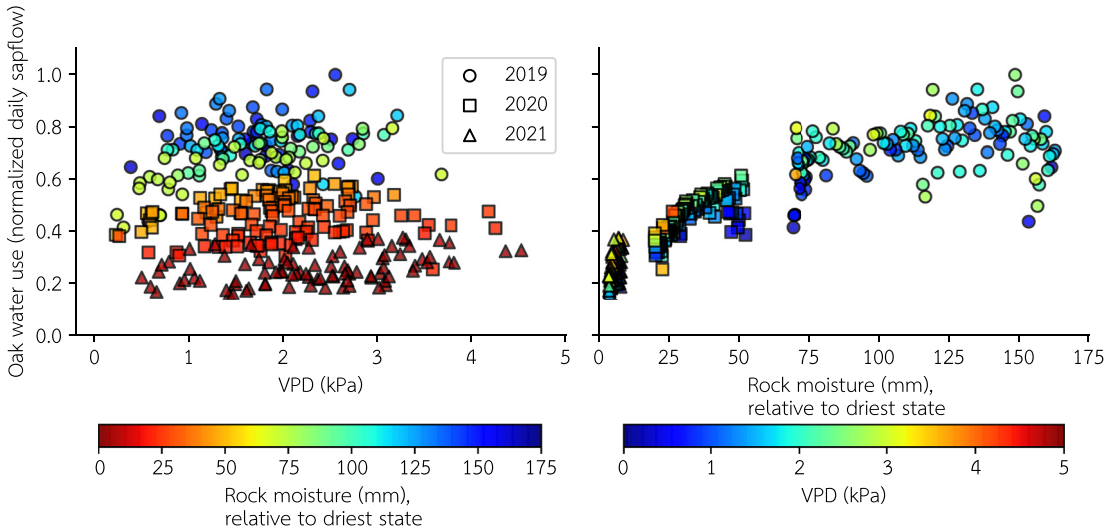

Figure 12. June 1 to September 30 daily blue oak water use (based on normalized daily sapflow) as a function of (a) atmpsheric water demand, expressed as vapor pressure deficit (VPD), and (b) site-wide average rock moisture availability (expressed relative to its driest state, sampled from the interpolated timeseries shown in Figure 10c). The same data is shown in both plots, but with the abscissa switched with the color bar. Symbol shape refers to year.

variance ($R^2 = 0.037$), whereas rock moisture explained a large fraction of the variance in sapflow ($R^2 = 0.798$). Multiple linear regression considering both terms together performed only marginally better than rock moisture alone ($R^2 = 0.801$). Collectively, these patterns support the hypothesis that water content in the weathered bedrock vadose zone is a first order control on oak water use in the summer dry season. The lack of meaningful control by VPD indicates that the site is strongly water-limited rather than energy-limited during the the summer.

Figure 13 plots cumulative June-September oak sapflow as a function of cumulative rock moisture depletion. If, during this time period, oak transpiration were drawn exclusively from the weathered bedrock vadose zone, and other fluxes into and out of that zone were negligible, the relationship would be linear. Both 2019 and 2020 exhibit an approximately linear relationship for most of the summer dry season, with a slightly higher amount of oak sapflow relative to rock moisture drawdown in September. In 2021, the relationship was also linear, but steeper than 2019 and 2020. These patterns are consistent with oak transpiration being sourced from the weathered bedrock vadose zone and driving the decline in rock moisture. Cumulative sapflow and rock moisture drawdown were both lower in the drought (2020 and 2021) years than in the initial wet (2019) year, consistent with the oak transpiration flux driving the change in storage of the rock moisture reservoir. We hypothesize that the increase in slope between individual years over the course of the drought is likely due to increased relative reliance of the oaks on the soil moisture reservoir, which—unlike the rock moisture reservoir—is partially filled during dry years.

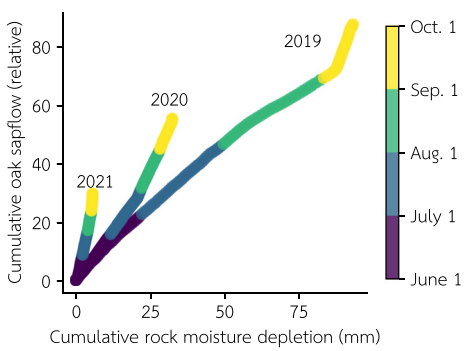

Figure 13. June 1 to September 30 cumulative blue oak water use, expressed as relative average sapflow (unitless), versus seasonal rock moisture depletion (drawdown), inferred from the neutron-probe based interpolated site-wide timeseries shown in Figure 10c.

3.8. Saturated Zone and Surface Water Dynamics

A deep, permanent saturated zone was observed under the three study ridgetops throughout the monitoring period. Under the two smaller hillslopes, which have local ridge-top reliefs of 25–28 m, groundwater lies between 15 and 21 m below the surface (boreholes MH3W1 and MH3W5). Under the larger MH7 hillslope, which has nearly twice the relief and ridge-valley spacing as the MH3 hillslopes, groundwater lies between 30 and 35 m below the surface (Figure 14b). Storms in the 2019 water year resulted in water level rises and recessions in all of these boreholes, indicative of recharge to the saturated zone beneath the ridges (note: water introduced during drilling in November 2018, caused an artifactual water level rise/recession in each borehole, which is denoted by the shaded region in Figure 14). The spring 2019 ridgetop groundwater responses occurred within 2–4 days of rainfall events. Following the last event, an extended groundwater level recession occurred,

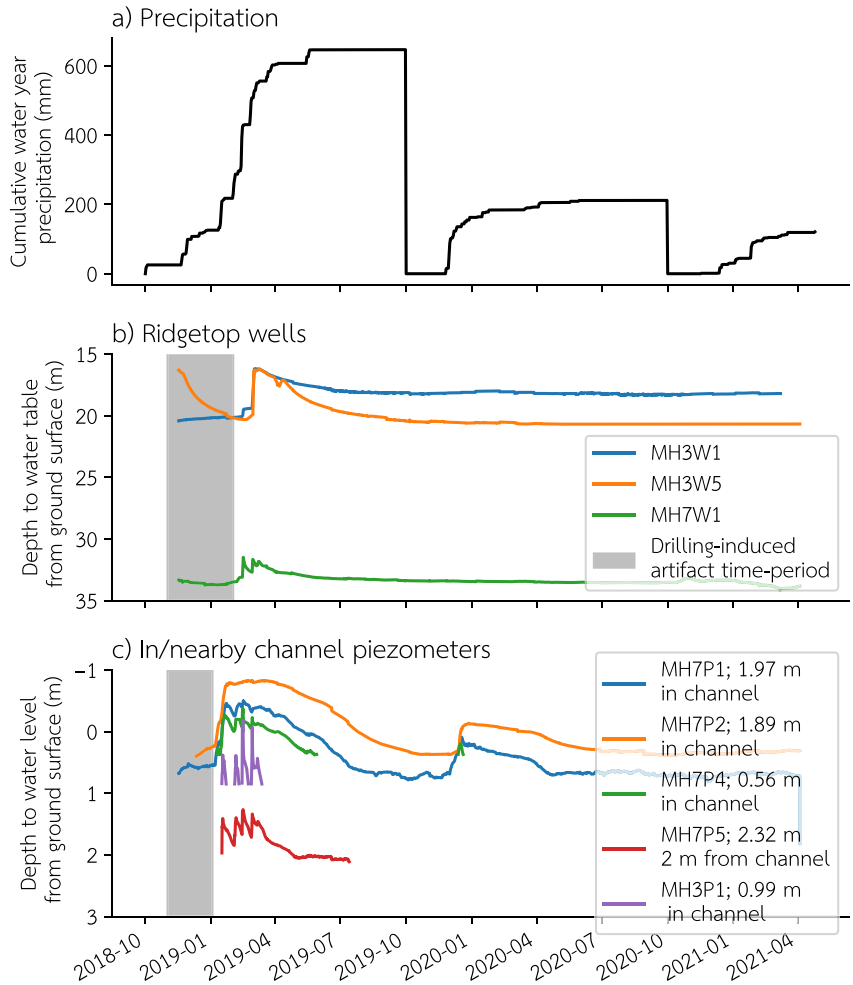

Figure 14. (a) Precipitation inputs to the site as recorded by the rain gauge at the MH catchment mouth. (b) Water level responses in screened wells at three ridge-tops. Initial shaded region denotes artifactual water level dynamic induced by drilling. Small step-offsets (<10 cm) are due to slight differences in vertical pressure transducer locations when they were removed and replaced during data download. (c) Water level responses in piezometers located in/near channel (see comments in legend). Missing data denotes times when water level receded below the transducer. Numbers in legend refer to depth of bottom of piezometer opening from ground surface.

spanning not just the subsequent dry season but the following two (relatively dry) wet seasons of the 2020 and 2021 water years (a likely artifactual groundwater rise is visible at the start of 2021 water year, which is likely due to a transducer depth placement error; no precipitation occurred to have driven this signal).

3.8.1. Piezometer Responses

Piezometers in mid-to up-slope positions (map in Figure 1) around the MH3 subcatchment were instrumented early in the 2019 water year to capture any near-surface saturated zone dynamic. Although the intense 2019 rainfall events led to landslides, recharge at the ridges (as shown in Figure 14), and streamflow, these piezometers stayed dry: the 0.4–2.3 m depth range at these locations remained unsaturated.

In contrast, valley-bottom and in-channel piezometers recorded shallow saturated zone dynamics. A 2.3 m deep piezometer situated in the MH7 valley bottom (MH7P5), 3 m above and laterally away from the channel, recorded 5 distinct saturated pressure head pulses in the 2019 WY, and then a recession through the summer before going dry (Figure 14c). The water level in the piezometer remained >1 m below the surface at all times. In the 2020 water year, only one small, ephemeral rise during a large November storm event occurred, and no dynamic was observed in the 2021 water year.

A 1 m deep, in-channel piezometer in the MH3 valley bottom similarly recorded 5 distinct events in the 2019 water year, with two events resulting in artesian head conditions (water levels in the piezometer rising above the ground surface). The three piezometers in the MH7 channel were installed with openings at different depths to capture vertical head gradients (2.1, 1.9, and 0.5 m, respectively, for MH7P2, MH7P1, and MH7P4). Each of these in-channel piezometers recorded multiple events in the 2019 WY, one event early in the 2020 WY, and none in the 2021 WY (Figure 14c). All the in-channel piezometers experienced sustained periods of artesian head conditions. The two deeper piezometers always remained saturated at the depth of the pressure transducer and had a smoother rise and recession than observed in other boreholes at the site, which tended to be flashier. Total head gradients indicated a component of vertically upward flow from 1.9 m depth to the bed of the bedrock channel.

3.8.2. Streamflow

Streamflow occurred throughout the geomorphic channel network in the wet 2019 WY, and persisted for days after rain events. After the storms, field excursions indicated that small springs sustained flow in the channels and originated where bedrock fractures intersected the ground surface along the channel banks and in convergent areas above channel heads. No significant ground surface saturation outside of the channel network was observed after rainfall events in the Mountain House catchment, consistent with the lack of observed near-surface saturation in the up-slope piezometers. The stage gauges installed at the MH3 and MH7 subcatchments on December 18, 2019 indicated that there was no streamflow through the remainder of the 2020 WY and the entirety of the extreme drought 2021 WY. Based on channel piezometer responses, there was likely some streamflow during the very first heavy storm event of the 2020 WY, prior to the stage gauge installation.

4. Discussion

We found that trees relied on rock moisture for transpiration in the summer dry season at a hilly Mediterranean oak savanna underlain by a thick weathered bedrock vadose zone. When 2 years of meteorological drought arrived, rock moisture was not fully replenished in winter, resulting in progressively lower summer water content in the subsurface and decreased tree water availability. This resulted in lower sapflow, lower water potentials earlier in the dry season, and—in the second year —reductions in leaf area due to smaller leaf size and canopy dieback. Our observations indicate that the bedrock water storage capacity was large relative to net precipitation in dry years. Under such precipitation-limited storage conditions, bedrock could not buffer the trees from a multi-year period of low precipitation: the meteorological drought became a root-zone drought. Furthermore, because infiltrating precipitation must transit a thick vadose zone before reaching the saturated zone, in the second year of low precipitation no groundwater recharge or streamflow occurred: all infiltrating precipitation was intercepted by the dry soil and weathered bedrock vadose zones. Finally, groundwater did not appear to be a significant water source for trees residing on the hillslopes, based on the great depth to the water table and the lack of dry season water table drawdowns.

Below, we discuss our findings in the context of storage capacity-based ecohydrologic frameworks and woody plant use of rock moisture.

4.1. Storage Capacity-Based Ecohydrologic Framework

We predicted that seasonal water storage would scale with winter precipitation, based on the relatively low mean annual precipitation at the site and previous observations by Pedrazas et al. (2021) of a thick, porous weathered bedrock zone with potential for high plant-available water storage capacity (Hahm, Rempe, et al., 2019). This finding would be consistent with seasonal water storage at the site being limited by precipitation rather than storage capacity (Fellows & Goulden, 2017; Hahm, Dralle, et al., 2019). We observed that seasonal rock moisture storage in the weathered bedrock vadose zone and groundwater levels were indeed higher in years with higher precipitation (Figure 10).

Precipitation-limited conditions and concomitant ecohydrological outcomes are likely not unique to Rancho Venada. Blue oak, a California endemic (and the largest oak community in the state), is distributed in a ring in the foothills surrounding the Central Valley, with a mean annual precipitation throughout the species range of 480 mm (Baldocchi & Xu, 2007; Xu & Baldocchi, 2003). Because blue oak savannas are typically found in semi-arid (relatively dry) locations, they may be more likely to experience precipitation-limited rather than

storage-capacity-limited conditions (because, all else equal, annual precipitation is low). If so, this should lead to relatively higher inter-annual variability (and precipitation dependence) of dry season water availability, transpiration, and productivity. This is consistent with observations at an intensively studied blue oak savanna on the eastern side of the Central Valley (Tonzi Ranch), across from our study site on the west, where more than a decade of eddy flux tower-based measurements show that ET is higher when groundwater depths are shallower in wet years (Baldocchi et al., 2021; Ma et al., 2007). Blue oaks also exhibit phenological responses suggestive of adaptation to variations in water supply, commonly shrinking leaf size (Weitz, 2018) and/or shedding leaves early (drought deciduous behavior; McDonald, 1990) in response to reductions in water availability. In spite of these adaptations, in the previous extreme California drought (2012–2016), 20% of the canopy of blue oaks in Sequoia National Park appeared to have died (Das et al., 2020). In the same drought, McLaughlin et al. (2020) found that blue oak canopy dieback percentage was negatively correlated with precipitation, and Huesca et al. (2021) found that blue oak canopy dieback was higher on south facing aspects (where higher insolation may increase summer water demand relative to north-facing slopes). (At our site, the oaks are absent from south-facing slopes.) Long-term evidence of blue oak sensitivity to wet season precipitation is found in tree ring chronologies (Stahle et al., 2013).

The precipitation-limited conditions that likely prevail across much of the range of blue oak stand in contrast to two other intensively studied sites—Rivendell and Sagehorn—north-west of Rancho Venada. These sites are also situated in the Northern California Coast Range, and host woody plant communities on hillslopes underlain by weathered bedrock mantled with thin soil. However, they experience on average four-times more annual rainfall (2,042 mm and 1,811 mm compared to 534 mm at Rancho Venada). At Rivendell and Sagehorn (a mixed broadleaf-coniferous evergreen forest and a deciduous oak savanna, respectively), comparable relative reductions in rainfall in the previous major California drought did not result in lower seasonal water storage, because net winter rainfall was still sufficient to replenish subsurface water storage (Hahm, Dralle, et al., 2019), which averages 472 mm at Rivendell and 102 mm at Sagehorn in winter (Dralle et al., 2018). Due to these storage capacity limited conditions, meteorological drought did not result in greater tree water stress at those sites in the drought and no canopy dieback was observed (Hahm et al., 2018; Rempe & Dietrich, 2018), even in locations where ET is higher (e.g., approximately 650 mm/yr at Rivendell). In Spain, which also experiences a rain-dominated Mediterranean climate, the coupling between annual vegetation greenness and a commonly used standardized precipitation index (a metric of meterological drought) was stronger at drier sites (Peña-Gallardo et al., 2018), which is also consistent with the increased likelihood of precipitation-limitation conditions. At a global level, recent meta-analysis has indicated that there is widespread drought-induced die-off at dry range edges (W. R. L. Anderegg et al., 2019), indicating that adaptations to xeric environments are incapable of buffering species' populations from extreme shortages of rainfall.

At other precipitation-limited sites in the Sierra Nevada, California, eddy covariance-measured ET and local precipitation records have been used to document not only the lack of storage replenishment through the previous extreme drought, but up to 1,500 mm of moisture overdraft (the highest amount by which cumulative ET exceeded P over the observed time period), which was argued to be sourced from deeply weathered bedrock (Goulden & Bales, 2019). Our in situ observations of dynamic rock moisture content also revealed a drawdown of moisture to a progressively lower state each year of drought (Figure 10).

4.2. Woody Plant Use of Bedrock Water

During the dry season at Rancho Venada, deep hillslope groundwater changes are negligible even in wet years (Figure 14), no streamflow occurs, and herbaceous groundcover is dead. Oak sapflow continues, however (Figure 7), and the tree transpiration rate is positively correlated with rock moisture availability (Figure 12). During our observations, cumulative water use by upper hillslope oaks was linearly related to cumulative dry season rock moisture drawdown (Figure 13). Furthermore, pre-dawn oak water potentials were extremely low (Figure 9), inconsistent with access to groundwater. Collectively, these observations indicate that declines in rock moisture content are driven by tree water uptake, and that trees rely on bedrock vadose zone storage to sustain dry season transpiration. This finding adds to a growing body of work that pinpoints the weathered bedrock vadose zone as a key woody plant water source, particularly in hilly landscapes that experience seasonally dry climates (Anderson et al., 1995; Arkley, 1981; Hahm et al., 2020; Hubbert et al., 2001; McCormick et al., 2021; Rempe & Dietrich, 2018; Rose et al., 2003; Witty et al., 2003; Zwieniecki & Newton, 1996). The observation that rock

moisture content is a better predictor of sapflow than VPD in the summer dry season indicates that bedrock vadose zone moisture dynamics should be considered in modeling contexts, particularly in similar water-limited contexts. Traditionally, most models have restricted transpiration to be a function of atmospheric water demand or energy supply and soil moisture, rather than the deeper bedrock vadose zone which may be more relevant.

Manzanita, which are also present but at a relatively small concentration at Rancho Venada, have been previously observed to extract moisture from the weathered bedrock vadose zone (Rose et al., 2003). In a classic study, Lewis and Burgy (1964) injected tritiated water into the saturated zone to infer groundwater uptake by blue oak and rooting depths in excess of 24 m. Miller et al. (2010), working at Tonzi Ranch, inferred groundwater uptake by blue oak roots >8 m below ground based primarily on strong diurnal oscillations in groundwater. Miller et al. (2010) suggested that blue oaks should be considered obligate phreatophytes and that groundwater use should buffer the oaks from meteorological drought. These studies did not specifically investigate water uptake from the weathered bedrock unsaturated zone, through which roots must have extended to reach deeper groundwater. We therefore hypothesize that oaks in these studies may have also used bedrock vadose zone storage, in addition to groundwater. Oaks studied at Tonzi had access to a shallower groundwater table (which can rise to just 3 m below the surface in the wet season). It is likely the case that blue oaks are opportunistic subsurface water users: where groundwater is inaccessible, particularly in upslope positions where the water table is at great depth and/or resides in potentially anoxic, low conductivity fresh bedrock, the oaks can survive on vadose zone moisture. In the upslope positions in the foothills of the Central Valley where bedrock is common, rock moisture is likely a significant component of the vadose zone plant-available water budget. In topographically convergent zones where groundwater may be nearer the surface and flowing through more conductive material, the oaks likely supplement their water supply with groundwater, and behave as phreatophytes. More study is needed to better understand the conditions under which unsaturated versus saturated water reservoirs are tapped. In locations with deep rooting, the traditionally monitored first 100 cm of the subsurface is likely inadequate to accurately describe plant water uptake and moisture availability.

5. Conclusion

Two years of extreme drought at Rancho Venada in the eastern Northern California Coast Range had cascading effects on the hillslope hydrologic cycle, impacting transpiration, recharge, and streamflow. Under the local Mediterranean climate, woody plants rely on rain that arrives in the wet season and is stored in the subsurface for dry season transpiration. Due to a deep weathering front and semi-arid climate, we predicted that subsurface water storage capacity would be greater than net winter precipitation (winter rainfall less evapotranspiration) in dry years, and that therefore storage would be variably replenished between years, causing precipitation-limited storage conditions and the potential for meteorological drought to decrease dry season plant water availability. This occurred through the 2020–2021 extreme drought, in which rock moisture storage in the thick weathered bedrock vadose zone was never fully replenished and experienced a multi-year net drawdown. Dry season tree water potential and transpiration were subsequently reduced, and in the second year of drought reduced leaf sizes and branch dieback were observed. Furthermore, because the dry weathered bedrock vadose zone intercepted the scant precipitation that infiltrated past the soil, no groundwater recharge or streamflow occurred. Collectively, our findings point to the importance of water storage dynamics throughout the weathered profile in hilly landscapes—which are commonly underlain by bedrock—for understanding the impact of drought on plant communities, groundwater recharge, and streamflow generation. Although trees at the site are rooted into and rely on water from the thick weathered bedrock vadose zone, access to rock moisture did not shield the trees from meteorological drought. The bedrock's large water storage capacity relative to precipitation in dry years resulted in decreased storage and lower plant-water availability that prompted a dieback episode. These findings motivate greater study of the distribution and water storage properties of weathered bedrock, and caution against the premise that large plant-available water storage capacity (including access to bedrock water) universally tends to buffer ecosystems from meteorological drought.

Data Availability Statement

Data and Python scripts used to process data and generate figures are hosted on Hydroshare: http://www.hydroshare.org/resource/aa8e4a74550f46e191f6f19d3adb740a/.

Acknowledgments
We are grateful to Jerry Brown, Anne Gust Brown, Rhonda Gruber, and Gregg Hemmi for site access and field support, numerous field assistants, including Kevin Mazzocco, for helping collect data, and Steve Taber for drilling boreholes. Funding sources for this project include Simon Fraser University, the Natural Sciences and Engineering Research Council of Canada, the Canadian Foundation for Innovation, the British Columbia Knowledge Development Fund, the US Department of Energy, Office of Science, Office of Biological Environmental Research under award number DESC0018039, the National Science Foundation supported Eel River Critical Zone Observatory (NSF EAR 1331940 and NSF EAR 2141763), the Carol Baird Graduate Student Award for Field Research, the University of California Institute for the Study of Ecological Effects of Climate Impacts, the University of California Berkeley Charles H. Ramsden Endowed Scholarship Fund, the Northern California Geological Society Richard Chambers Memorial Scholarship, the National Center for Airborne Laser Mapping, and the University of Texas Jackson School of Geosciences.

References

Allen, C. D., Macalady, A. K., Chenchouni, H., Bachelet, D., McDowell, N., Vennetier, M., et al. (2010). A global overview of drought and heat-induced tree mortality reveals emerging climate change risks for forests. *Forest Ecology and Management*, *259*(4), 660–684. https://doi.org/10.1016/j.foreco.2009.09.001

Amundson, R., Heimsath, A., Owen, J., Yoo, K., & Dietrich, W. E. (2015). Hillslope soils and vegetation. *Geomorphology*, *234*, 122–132. https://doi.org/10.1016/j.geomorph.2014.12.031

Anderegg, L. D. L., Anderegg, W. R. L., & Berry, J. A. (2013). Not all droughts are created equal: Translating meteorological drought into woody plant mortality. *Tree Physiology*, *33*(7), 672–683. https://doi.org/10.1093/treephys/tpt044

Anderegg, W. R. L., Anderegg, L. D. L., Kerr, K. L., & Trugman, A. T. (2019). Widespread drought-induced tree mortality at dry range edges indicates that climate stress exceeds species' compensating mechanisms. *Global Change Biology*, *25*(11), 3793–3802. https://doi.org/10.1111/gcb.14771

Anderson, M. A., Graham, R. C., Alyanakian, G. J., & Martynn, D. Z. (1995). Late summer water status of soils and weathered bedrock in a giant sequoia grove. *Soil Science*, *160*, 415–422. https://doi.org/10.1097/00010694-199512000-00007

Arkley, R. J. (1981). Soil moisture use by mixed conifer forest in a summer-dry climate. *Soil Science Society of America Journal*, *45*, 423–427. https://doi.org/10.2136/sssaj1981.03615995004500020037x

Baldocchi, D. D., Ma, S., & Verfaillie, J. (2021). On the inter- and intra-annual variability of ecosystem evapotranspiration and water use efficiency of an oak savanna and annual grassland subjected to booms and busts in rainfall. *Global Change Biology*, *27*(2), 359–375. https://doi.org/10.1111/gcb.15414

Baldocchi, D. D., & Xu, L. (2007). What limits evaporation from Mediterranean oak woodlands—The supply of moisture in the soil, physiological control by plants or the demand by the atmosphere? *Advances in Water Resources*, *30*(10), 2113–2122. https://doi.org/10.1016/j.advwatres.2006.06.013

Brantley, S. L., Eissenstat, D. M., Marshall, J. A., Godsey, S. E., Balogh-Brunstad, Z., Karwan, D. L., et al. (2017). Reviews and syntheses: On the roles trees play in building and plumbing the critical zone. *Biogeosciences*, *14*(22).

Breshears, D. D., Adams, H. D., Eamus, D., McDowell, N., Law, D. J., Will, R. E., et al. (2013). The critical amplifying role of increasing atmospheric moisture demand on tree mortality and associated regional die-off. *Frontiers of Plant Science*, *4*, 266.

Choat, B., Brodribb, T. J., Brodersen, C. R., Duursma, R. A., Lopez, R., & Medlyn, B. E. (2018). Triggers of tree mortality under drought. *Nature*, *558*(7711), 531–539.

Crouchet, S. E., Jensen, J., Schwartz, B. F., & Schwinning, S. (2019). Tree mortality after a hot drought: Distinguishing density-dependent and-independent drivers and why it matters. *Frontiers in Forests and Global Change*, *2*, 21.

Das, A. J., Ampersee, N. J., Pfaff, A. H., Stephenson, N. L., Swiecki, T. J., Bernhardt, E. A., et al. (2020). Tree mortality in blue oak woodland during extreme drought in Sequoia National Park, California. *Madroño*, *66*(4), 164–175. https://doi.org/10.3120/0024-9637-66.4.164

Dawson, T. E., Hahm, W. J., & Crutchfield-Peters, K. (2020). Digging deeper: What the critical zone perspective adds to the study of plant ecophysiology. *New Phytologist*, *226*, 666–671. https://doi.org/10.1111/nph.16410

Dettinger, M. D., Ralph, F. M., Das, T., Neiman, P. J., & Cayan, D. R. (2011). Atmospheric rivers, floods and the water resources of California. *Water*, *3*(2), 445–478. https://doi.org/10.3390/w3020445

Ding, Y., Nie, Y., Chen, H., Wang, K., & Querejeta, J. I. (2020). Water uptake depth is coordinated with leaf water potential, water-use efficiency and drought vulnerability in karst vegetation. *New Phytologist*, *229*(3), 1339–1353.

Dralle, D. N., Hahm, W. J., Rempe, D. M., Karst, N. J., Thompson, S. E., & Dietrich, W. E. (2018). Quantification of the seasonal hillslope water storage that does not drive streamflow: Catchment storage that does not drive streamflow. *Hydrological Processes*, *32*. https://doi.org/10.1002/hyp.11627

Entekhabi, D., Njoku, E. G., O'Neill, P. E., Kellogg, K. H., Crow, W. T., Edelstein, W. N., et al. (2010). The soil moisture active passive (SMAP) mission. *Proceedings of the IEEE*, *98*(5), 704–716. https://doi.org/10.1109/JPROC.2010.2043918

Fellows, A. W., & Goulden, M. L. (2017). Mapping and understanding dry season soil water drawdown by California montane vegetation. *Ecohydrology*, *10*(1), e1772. https://doi.org/10.1002/eco.1772

Forster, M. A. (2019). The dual method approach (DMA) resolves measurement range limitations of heat pulse velocity sap flow sensors. *Forests*, *10*(1), 46. https://doi.org/10.3390/f10010046

Gorelick, N., Hancher, M., Dixon, M., Ilyushchenko, S., Thau, D., & Moore, R. (2017). Google Earth engine: Planetary-scale geospatial analysis for everyone. *Remote Sensing of Environment*, *202*, 18–27.

Goulden, M. L., & Bales, R. C. (2019). California forest die-off linked to multi-year deep soil drying in 2012–2015 drought. *Nature Geoscience*, *12*(8), 632–637.

Graham, R., Rossi, A., & Hubbert, R. (2010). Rock to regolith conversion: Producing hospitable substrates for terrestrial ecosystems. *Geological Society of America Today*, *20*(2), 4–9. https://doi.org/10.1130/GSAT57A.1

Hahm, W. J., Dietrich, W., & Dawson, T. (2018). Controls on the distribution and resilience of Quercus garryana: Ecophysiological evidence of oak's water-limitation tolerance. *Ecosphere*, *9*(5), e02218. https://doi.org/10.1002/ecs2.2218

Hahm, W. J., Dralle, D. N., Rempe, D. M., Bryk, A. B., Thompson, S. E., Dawson, T. E., & Dietrich, W. E. (2019). Low subsurface water storage capacity relative to annual rainfall decouples mediterranean plant productivity and water use from rainfall variability. *Geophysical Research Letters*, *46*, 6544–6553. https://doi.org/10.1029/2019gl083294

Hahm, W. J., Rempe, D. M., Dralle, D. N., Dawson, T. E., & Dietrich, W. E. (2020). Oak transpiration drawn from the weathered bedrock vadose zone in the summer dry season. *Water Resources Research*, *56*(11), e2020WR027419. https://doi.org/10.1029/2020WR027419

Hahm, W. J., Rempe, D. M., Dralle, D. N., Dawson, T. E., Lovill, S. M., Bryk, A. B., et al. (2019). Lithologically controlled subsurface critical zone thickness and water storage capacity determine regional plant community composition. *Water Resources Research*, *55*, 3028–3055. https://doi.org/10.1029/2018wr023760

Huang, M.-H., Hudson-Rasmussen, B., Burdick, S., Lekic, V., Nelson, M. D., Fauria, K. E., & Schmerr, N. (2021). Bayesian seismic refraction inversion for critical zone science and near-surface applications. *Geochemistry, Geophysics, Geosystems*, *22*(5), e2020GC009172. https://doi.org/10.1029/2020GC009172

Hubbert, K., Beyers, J., & Graham, R. (2001). Roles of weathered bedrock and soil in seasonal water relations of Pinus Jeffreyi and Arctostaphylos patula. *Canadian Journal of Forest Research*, *31*, 1947. https://doi.org/10.1139/cjfr-31-11-1947

Huesca, M., Ustin, S. L., Shapiro, K. D., Boynton, R., & Thorne, J. H. (2021). Detection of drought-induced blue oak mortality in the Sierra Nevada Mountains, California. *Ecosphere*, *12*(6), e03558. https://doi.org/10.1002/ecs2.3558

Huete, A., Didan, K., Miura, T., Rodriguez, E. P., Gao, X., & Ferreira, L. G. (2002). Overview of the radiometric and biophysical performance of the MODIS vegetation indices. *Remote Sensing of Environment*, *83*(1–2), 195–213. https://doi.org/10.1016/S0034-4257(02)00096-2

Ichii, K., Wang, W., Hashimoto, H., Yang, F., Votava, P., Michaelis, A. R., & Nemani, R. R. (2009). Refinement of rooting depths using satellite-based evapotranspiration seasonality for ecosystem modeling in California. *Agricultural and Forest Meteorology*, *149*(11), 1907–1918.

Immerzeel, W. W., Lutz, A. F., Andrade, M., Bahl, A., Biemans, H., Bolch, T., et al. (2020). Importance and vulnerability of the world's water towers. *Nature*, *577*(7790), 364–369. https://doi.org/10.1038/s41586-019-1822-y

Jump, A. S., Ruiz-Benito, P., Greenwood, S., Allen, C. D., Kitzberger, T., Fensham, R., et al. (2017). Structural overshoot of tree growth with climate variability and the global spectrum of drought-induced forest dieback. *Global Change Biology*, *23*(9), 3742–3757. https://doi.org/10.1111/gcb.13636

Klos, P. Z., Goulden, M. L., Riebe, C. S., Tague, C. L., O'Geen, A. T., Flinchum, B. A., et al. (2018). Subsurface plant-accessible water in mountain ecosystems with a Mediterranean climate. *WIREs Water*, *5*, e1277.

Kottek, M., Grieser, J., Beck, C., Rudolf, B., & Rubel, F. (2006). World Map of the Köppen-Geiger climate classification updated. *Meteorologische Zeitschrift*, 259–263. https://doi.org/10.1127/0941-2948/2006/0130

Laio, F., Porporato, A., Ridolfi, L., & Rodriguez-Iturbe, I. (2001). Plants in water-controlled ecosystems: Active role in hydrologic processes and response to water stress: II. Probabilistic soil moisture dynamics. *Advances in Water Resources*, *24*(7), 707–723. https://doi.org/10.1016/S0309-1708(01)00005-7

Lewis, D. C., & Burgy, R. H. (1964). The Relationship between oak tree roots and groundwater in fractured rock as determined by tritium tracing. *Journal of Geophysical Research*, *69*, 2579–2588. https://doi.org/10.1029/JZ069i012p02579

Liu, Y., Hill, M. J., Zhang, X., Wang, Z., Richardson, A. D., Hufkens, K., et al. (2017). Using data from Landsat, MODIS, VIIRS and PhenoCams to monitor the phenology of California oak/grass savanna and open grassland across spatial scales. *Agricultural and Forest Meteorology*, *237–238*, 311–325. https://doi.org/10.1016/j.agrformet.2017.02.026

Long, I. F., & French, B. K. (1967). Measurement of soil moisture in the field by neutron moderation. *Journal of Soil Science*, *18*(1), 149–166. https://doi.org/10.1111/j.1365-2389.1967.tb01496.x

Ma, S., Baldocchi, D. D., Xu, L., & Hehn, T. (2007). Inter-annual variability in carbon dioxide exchange of an oak/grass savanna and open grassland in California. *Agricultural and Forest Meteorology*, *147*(3), 157–171. https://doi.org/10.1016/j.agrformet.2007.07.008

Mackay, D. S., Savoy, P. R., Grossiord, C., Tai, X., Pleban, J. R., Wang, D. R., et al. (2020). Conifers depend on established roots during drought: Results from a coupled model of carbon allocation and hydraulics. *New Phytologist*, *225*(2), 679–692.

McCormick, E. L., Dralle, D. N., Hahm, W. J., Tune, A. K., Schmidt, L. M., Chadwick, K. D., & Rempe, D. M. (2021). Widespread woody plant use of water stored in bedrock. *Nature*, *597*(7875), 225–229. https://doi.org/10.1038/s41586-021-03761-3

McDonald, P. M. (1990). Quercus douglasii Hook. & Arn. Blue oak. In *Silvics of North America: Hardwoods* (Vol. 2, p. 877). United States Department of Agriculture, Forest Service.

McDowell, N. G., Grossiord, C., Adams, H. D., Pinzón-Navarro, S., Mackay, D. S., Breshears, D. D., et al. (2019). Mechanisms of a coniferous woodland persistence under drought and heat. *Environmental Research Letters*, *14*(4), 045014

McLaughlin, B. C., Ackerly, D. D., Klos, P. Z., Natali, J., Dawson, T. E., & Thompson, S. E. (2017). Hydrologic refugia, plants, and climate change. *Global Change Biology*, *23*(8), 2941–2961. https://doi.org/10.1111/gcb.13629

McLaughlin, B. C., Blakey, R., Weitz, A. P., Feng, X., Brown, B. J., Ackerly, D. D., et al. (2020). Weather underground: Subsurface hydrologic processes mediate tree vulnerability to extreme climatic drought. *Global Change Biology*, *26*(5), 3091–3107. https://doi.org/10.1111/gcb.15026

Miller, G. R., Chen, X., Rubin, Y., Ma, S., & Baldocchi, D. D. (2010). Groundwater uptake by woody vegetation in a semiarid oak savanna. *Water Resources Research*, *46*. https://doi.org/10.1029/2009wr008902

Milly, P. C. D. (1994). Climate, interseasonal storage of soil water, and the annual water balance. *Advances in Water Resources*, *17*(1), 19–24. https://doi.org/10.1016/0309-1708(94)90020-5

Nardini, A., Petruzzellis, F., Marusig, D., Tomasella, M., Natale, S., Altobelli, A., et al. (2020). Water 'on the rocks': A summer drink for thirsty trees? *New Phytologist*, *14*.

Nourtier, M., Chanzy, A., Cailleret, M., Yingge, X., Huc, R., & Davi, H. (2014). Transpiration of silver Fir (Abies alba mill.) during and after drought in relation to soil properties in a Mediterranean mountain area. *Annals of Forest Science*, *71*(6), 683–695. https://doi.org/10.1007/s13595-012-0229-9

Pedrazas, M. A., Hahm, W. J., Huang, M.-H., Dralle, D., Nelson, M. D., Breunig, R. E., et al. (2021). The relationship between topography, bedrock weathering, and water storage across a sequence of ridges and valleys. *Journal of Geophysical Research: Earth Surface*, *126*(4), e2020JF005848. https://doi.org/10.1029/2020JF005848

Peña-Gallardo, M., Vicente-Serrano, S. M., Camarero, J. J., Gazol, A., Sánchez-Salguero, R., Domínguez-Castro, F., et al. (2018). Drought sensitiveness on forest growth in peninsular Spain and the Balearic Islands. *Forests*, *9*(9), 524. https://doi.org/10.3390/f9090524

Porporato, A., Daly, E., & Rodriguez-Iturbe, I. (2004). Soil water balance and ecosystem response to climate change. *The American Naturalist*, *164*, 625–632. https://doi.org/10.1086/424970

PRISM Climate Group. (2021). *PRISM climate data* (Tech. Rep.). Oregon State University. Retrieved from http://prism.oregonstate.edu

Rempe, D. M., & Dietrich, W. E. (2018). Direct observations of rock moisture, a hidden component of the hydrologic cycle. *Proceedings of the National Academy of Sciences*, *115*(11), 2664–2669.

Rich, E. I., (1971). *Geologic map of the Wilbur Springs Quadrangle, Colusa and Lake counties*. IMAP. https://doi.org/10.3133/i538

Riebe, C. S., Hahm, W. J., & Brantley, S. L. (2017). Controls on deep critical zone architecture: A historical review and four testable hypotheses. *Earth Surface Processes and Landforms*, *42*, 128–156. https://doi.org/10.1002/esp.4052

Roche, J. W., Ma, Q., Rungee, J., & Bales, R. C. (2020). Evapotranspiration mapping for forest management in California's sierra Nevada. *Frontiers in Forests and Global Change*, *3*, 69. https://doi.org/10.3389/ffgc.2020.00069

Rose, K., Graham, R., & Parker, D. (2003). Water source utilization by Pinus jeffreyi and Arctostaphylos patula on thin soils over bedrock. *Oecologia*, *134*(1), 46–54. https://doi.org/10.1007/s00442-002-1084-4

Ryu, Y., Baldocchi, D. D., Kobayashi, H., van Ingen, C., Li, J., Black, T. A., et al. (2011). Integration of MODIS land and atmosphere products with a coupled-process model to estimate gross primary productivity and evapotranspiration from 1 km to global scales. *Global Biogeochemical Cycles*, *25*(4), GB4017. https://doi.org/10.1029/2011GB004053

Salve, R., Rempe, D. M., & Dietrich, W. E. (2012). Rain, rock moisture dynamics, and the rapid response of perched groundwater in weathered, fractured argillite underlying a steep hillslope. *Water Resources Research*, *48*(11), W11528. https://doi.org/10.1029/2012WR012583

Sanders, M., Nelson, M. D., Bryk, A. B., Huang, M. H., Fauria, K., & Dietrich, W. E. (2019). The role of small shallow landslides in landscape evolution as revealed by high resolution differential lidar surveys and field mapping. In *Agu fall meeting abstracts* (Vol. 2019, p. EP43D-2399).

Sayama, T., McDonnell, J. J., Dhakal, A., & Sullivan, K. (2011). How much water can a watershed store? *Hydrological Processes*, *25*(25), 3899–3908. https://doi.org/10.1002/hyp.8288

Sazib, N., Mladenova, I., & Bolten, J. (2018). Leveraging the Google Earth engine for drought assessment using global soil moisture data. *Remote Sensing*, *10*(8), 1265. https://doi.org/10.3390/rs10081265

Schmidt, L., & Rempe, D. (2020). Quantifying dynamic water storage in unsaturated bedrock with borehole nuclear magnetic resonance. *Geophysical Research Letters*, *47*(22). e2020GL089600. https://doi.org/10.1029/2020GL089600

Scholander, P. F., Bradstreet, E. D., Hemmingsen, E., & Hammel, H. (1965). Sap pressure in vascular plants: Negative hydrostatic pressure can be measured in plants. *Science*, *148*(3668), 339–346.

Schwinning, S. (2020). A critical question for the critical zone: How do plants use rock water? *Plant and Soil*, *454*, 49–56. https://doi.org/10.1007/s11104-020-04648-4

Smith, T. J., McNamara, J. P., Flores, A. N., Gribb, M. M., Aishlin, P. S., & Benner, S. G. (2011). Small soil storage capacity limits benefit of winter snowpack to upland vegetation. *Hydrological Processes*, *25*(25), 3858–3865. https://doi.org/10.1002/hyp.8340

Snyder, R. (2005). *The ASCE standardized reference evapotranspiration equation* (Tech. Rep. No. 173). ASCE.

Soil Survey Staff. (2018). *Soil Survey Geographic (SSURGO) database for California*. United States Department of Agriculture, Natural Resources Conservation Service.

Stahle, D. W., Griffin, R. D., Meko, D. M., Therrell, M. D., Edmondson, J. R., Cleaveland, M. K., et al. (2013). The ancient blue oak woodlands of California: Longevity and hydroclimatic history. *Earth Interactions*, *17*(12), 1–23. https://doi.org/10.1175/2013EI000518.1

Steinkamp, J., & Hickler, T. (2015). Is drought-induced forest dieback globally increasing? *Journal of Ecology*, *103*(1), 31–43. https://doi.org/10.1111/1365-2745.12335

Swain, D. L., Langenbrunner, B., Neelin, J. D., & Hall, A. (2018). Increasing precipitation volatility in twenty-first-century California. *Nature Climate Change*, *8*(5), 427–433. https://doi.org/10.1038/s41558-018-0140-y

Tague, C. L., & Moritz, M. A. (2019). Plant accessible water storage capacity and tree-scale root interactions determine how forest density reductions alter forest water use and productivity. *Frontiers in Forests and Global Change*, *2*, 36. https://doi.org/10.3389/ffgc.2019.00036

Tramblay, Y., Koutroulis, A., Samaniego, L., Vicente-Serrano, S. M., Volaire, F., Boone, A., et al. (2020). Challenges for drought assessment in the mediterranean region under future climate scenarios. *Earth-Science Reviews*, *210*, 103348. https://doi.org/10.1016/j.earscirev.2020.103348

Trugman, A. T., Anderegg, L. D., Anderegg, W. R., Das, A. J., & Stephenson, N. L. (2021). Why is tree drought mortality so hard to predict? *Trends in Ecology & Evolution*.

Tune, A. K., Druhan, J. L., Wang, J., Bennett, P. C., & Rempe, D. M. (2020). Carbon dioxide production in bedrock beneath soils substantially contributes to forest carbon cycling. *Journal of Geophysical Research: Biogeosciences*, *125*(12), e2020JG005795. https://doi.org/10.1029/2020JG005795

USFS. (2016). *2016 aerial survey results: California* (Tech. Rep. No. R5-PR-034). USDA. Retrieved from https://www.fs.usda.gov/detail/r5/forest-grasslandhealth/?cid=fsbdev3_046696

Wald, J. A., Graham, R. C., & Schoeneberger, P. J. (2013). Distribution and properties of soft weathered bedrock at 1 m depth in the contiguous United States. *Earth Surface Processes and Landforms*, *38*(6), 614–626.

Weitz, A. (2018). *The physiological ecology of Californian blue oak (Quercus douglasii) and valley oak (Quercus lobata) woodlands in response to extreme drought (Doctoral dissertation). UC Berkeley*. Retrieved from https://escholarship.org/uc/item/3x75z324

Williams, A. P., Allen, C. D., Macalady, A. K., Griffin, D., Woodhouse, C. A., Meko, D. M., et al. (2013). Temperature as a potent driver of regional forest drought stress and tree mortality. *Nature Climate Change*, *3*(3), 292–297.

Witty, J. H., Graham, R. C., Hubbert, K. R., Doolittle, J. A., & Wald, J. A. (2003). Contributions of water supply from the weathered bedrock zone to forest soil quality. *Geoderma*, *114*, 389–400. https://doi.org/10.1016/S0016-7061(03)00051-X

Wu, C., Yeh, P. J.-F., Chen, Y.-Y., Hu, B. X., & Huang, G. (2020). Future precipitation-driven meteorological drought changes in the cmip5 multimodel ensembles under 1.5°C and 2°C global warming. *Journal of Hydrometeorology*, *21*(9), 2177–2196.

Wu, Z., Behzad, H. M., He, Q., Wu, C., Bai, Y., & Jiang, Y. (2021). Seasonal transpiration dynamics of evergreen ligustrum lucidum linked with water source and water-use strategy in a limestone karst area, southwest China. *Journal of Hydrology*, *597*, 126199.

Xu, L., & Baldocchi, D. D. (2003). Seasonal trends in photosynthetic parameters and stomatal conductance of blue oak (Quercus douglasii) under prolonged summer drought and high temperature. *Tree Physiology*, *23*(13), 865–877. https://doi.org/10.1093/treephys/23.13.865

Zanardo, S., Harman, C., Troch, P., Rao, P., & Sivapalan, M. (2012). Intra-annual rainfall variability control on interannual variability of catchment water balance: A stochastic analysis. *Water Resources Research*, *48*(6)

Zwieniecki, M. A., & Newton, M. (1996). Water-holding characteristics of metasedimentary rock in selected forest ecosystems in southwestern Oregon. *Soil Science Society of America Journal*, *60*, 1578–1582. https://doi.org/10.2136/sssaj1996.03615995006000050042x